Europe PMC Funders Group
Author Manuscript
Bioconjug Chem. Author manuscript; available in PMC 2021 July 22.

Published in final edited form as:
Bioconjug Chem. 2021 July 21; 32(7): 1242–1254. doi:10.1021/acs.bioconjchem.0c00561.

Optimal His-Tag Design for Efficient $[^{99m}Tc(CO)_3]^+$ and $[^{188}Re(CO)_3]^+$ Labeling of Proteins for Molecular Imaging and Radionuclide Therapy by Analysis of Peptide Arrays

Jennifer D. Williams, **Florian Kampmeier**, **Adam Badar**
King's College London, School of Biomedical Engineering and Imaging Sciences, London SE1 7EH, United Kingdom

Kevin Howland
Biomolecular Science Facility, University of Kent, Canterbury CT2 7NJ, United Kingdom

Margaret S. Cooper, **Gregory E. D. Mullen**, **Philip J. Blower**
King's College London, School of Biomedical Engineering and Imaging Sciences, London SE1 7EH, United Kingdom

Abstract

Hexahistidine tags (His-tags), incorporated into recombinant proteins to facilitate purification using metal-affinity chromatography, are useful binding sites for radiolabeling with $[^{99m}Tc(CO)_3]^+$ and $[^{188}Re(CO)_3]^+$ for molecular imaging and radionuclide therapy. Labeling efficiencies vary unpredictably, and the method is therefore not universally useful. To overcome this, we have made quantitative comparisons of radiolabeling of a bespoke Celluspots array library of 382 His-tag-containing peptide sequences with $[^{99m}Tc(CO)_3]^+$ and $[^{188}Re(CO)_3]^+$ to identify key features that enhance labeling. A selected sequence with 10-fold enhanced labeling efficiency compared to the most effective literature-reported sequences was incorporated into an exemplar protein and compared biologically with non-optimized analogues, in vitro and in vivo. Optimal labeling with either $[^{99m}Tc(CO)_3]^+$ or $[^{188}Re(CO)_3]^+$ required six consecutive His residues in the protein sequence, surrounded by several positively charged residues (Arg or Lys), and the presence of phosphate in the buffer. Cys or Met residues in the sequence were beneficial, to a lesser extent. Negatively charged residues were deleterious to labeling. His-tags with adjacent positively charged residues could be labeled as much as 40 times more efficiently than those with adjacent negatively charged residues. ^{31}P NMR of $[Re(CO)_3(H_2O)_3]^+$ and electrophoresis of solutions of $[^{99m}Tc(CO)_3(H_2O)_3]^+$ suggest that phosphate bridges form between cationic residues and the cationic metal synthon during labeling. The trial optimized protein, a scFv targeted to the PSMA antigen expressed in prostate cancer, was readily labeled in >95% radiochemical yield, without the need for subsequent purification. Labeling occurred more quickly and to higher specific activity

Correspondence to: Philip J. Blower.

Corresponding Author: **Philip J. Blower –** King's College London, School of Biomedical Engineering and Imaging Sciences, London SE1 7EH, United Kingdom; Phone: +44 (0)207 188 9513; Philip.blower@kcl.ac.uk.

Author Contributions
The manuscript was written through contributions of all authors. All authors have given approval to the final version of the manuscript.

Notes
The authors declare no competing financial interest.

Europe PMC Funders Author Manuscripts
Europe PMC Funders Author Manuscripts

than comparable non-optimized proteins, while retaining specific binding to PSMA and prostate cancer in vivo. Thus, optimized His-tags greatly simplify radiolabeling of recombinant proteins making them potentially more widely and economically available for imaging and treating patients.

Introduction

Molecular imaging using radiolabeled recombinant proteins, such as engineered antibody fragments, offers great potential for personalized medicine. Despite the rise of positron emission tomography in the last two decades, and recent worldwide shortages of the gamma emitter technetium-99m (^{99m}Tc), the importance of ^{99m}Tc as the staple of nuclear medicine for almost half a century is undiminished. Major investments in new facilities for commercial production of ^{99m}Tc and its parent isotope molybdenum-99,[1] and improvements in SPECT imaging hardware,[2] are underway. With its ideal half-life and gamma emissions, ^{99m}Tc will retain its clinical role in years to come. Despite the simplicity with which conventional ^{99m}Tc radiopharmaceuticals are prepared (by simple addition of [^{99m}Tc][TcO_4]$^-$ eluted in saline from the generator into a “kit” vial containing lyophilized ingredients), methods for radiolabeling proteins remain relatively complex and inconvenient, severely limiting their general accessibility. Kit-based methodology for ^{99m}Tc-labeling of proteins that is simple to perform (sterile, one step, quick, quantitative, room temperature, without extremes of pH), compatible with good manufacturing practice (GMP) and giving a radiochemically homogeneous, high specific activity product that is stable *in vivo*, is an important goal.

A widely used and versatile method for labeling recombinant proteins with ^{99m}Tc exploits the kinetically inert binding of the [^{99m}Tc][$Tc(CO)_3$]$^+$ fragment to proteins incorporating a His-tag—a polyhistidine sequence consisting typically of six consecutive His residues often engineered at the N- or C-terminus to facilitate downstream purification by immobilized metal-affinity chromatography.[3] This elegant radiolabeling method, developed by Waibel et al.,[4,5] has been used to radiolabel many His-tagged proteins and is also applicable to the β^--emitting therapeutic congeners, ^{186}Re and ^{188}Re.[6,7]

Despite its widespread use in molecular imaging research (e.g., labeled Herceptin for breast cancer imaging and Annexin V for apoptosis imaging[8,9]), use of this method in humans remains rare, and no commercial products are available. This may be in part because its practical utility varies between proteins and is unpredictable, giving quantitative (i.e., >95%) radiochemical yield only rarely. The coordination chemistry of the interaction between the metal complex and the His-tag is poorly understood.[4,7,10] Despite the assumption that radiolabeling is specific to the His-tag, non-His-tagged proteins can be radiolabeled by this method, albeit with greatly reduced efficiency.[11] It was only recently demonstrated that labeling is indeed site-specific: the recombinant protein C2A (phosphatidylserine binding-domain of rat synaptotagmin I, which has no His-tag) was radiolabeled with ^{99m}Tc in 15% radiochemical yield, whereas a His-tagged variant could be labeled in 100% yield under the same conditions; moreover, LCMS analysis of a tryptic digest of conjugates of [$Re(CO)_3$]$^+$ with the His-tagged protein showed that only the His-tag-containing fragments were bound

Europe PMC Funders Author Manuscripts
Europe PMC Funders Author Manuscripts

Europe PMC Funders Author Manuscripts

Europe PMC Funders Author Manuscripts

to rhenium. Competitive coincubation of equimolar His-tagged (a-CD33 scFv, 29 kDa) and a non-His-tagged (C2Ac, 15 kDa) protein with $[^{99m}Tc][Tc\text{-}(CO)_3]^+$[12,13] showed that more than 98% of the proteinbound $[^{99m}Tc][Tc(CO)_3]^+$ was bound to the His-tagged protein, and less than 2% to the non-His-tagged protein C2Ac.[14] Mass spectrometry showed that no exogenous ligands other than the protein and three carbonyl ligands were bound to the metal.[7,13] A cysteine residue close to the His-tag improved labeling kinetics, and LCMS suggested that the cysteine participates directly alongside the His-tag in binding the metal.[15] Increasing ionic strength also appears to enhance reaction rate.[14]

A survey of available literature (see SI Table S1) shows that while some His-tagged proteins can be labeled efficiently with $[^{99m}Tc][Tc(CO)_3]^+$ under mild conditions, others require excessively high protein concentration, prolonged incubation, elevated temperature, and/or subsequent purification to reach radiochemical purities (>95%) adequate for biological use.[16] Clearly, then, a His-tag sequence in a protein is not in itself sufficient to guarantee efficient labeling; structural variation in and around the His-tag plays a significant but uncharacterized role. Characterizing the role of neighboring residues would thus help identify a general optimal sequence that would guarantee efficient labeling, enhancing clinical utility by underpinning a single-step kit-based formulation. Here, we describe a combinatorial approach to screen a large number of genetically encodable peptide sequences for binding to $[^{99m}Tc][Tc(CO)_3]^+$, using SPOT[17] peptide screening via a commercial platform known as Celluspots, a 48 × 16 planar array consisting of duplicates of 382 N-terminally acetylated peptides and two controls (unmodified cellulose and acetylated cellulose). Each (typically 15-mer) peptide is C-terminally covalently linked to the modified cellulose membrane covering a 26 × 67 mm^2 glass slide, with spots 1.2 mm apart. By radiolabeling the array with $[^{99m}Tc][Tc(CO)_3]^+$ and $[^{188}Re\text{-}(CO)_3]^+$ and quantifying the radioactivity of each spot using autoradiography, the radiolabeling characteristics of the peptides could be screened to identify a genetically encodable His-tag design with optimal radiolabeling properties. A sequence optimized in this way was evaluated in a model protein, and tested in *vivo*, compared with similar nonoptimized His-tagged proteins. The proteins included scFv antibody fragments targeting the prostate-specific membrane antigen (PSMA), which is currently of wide interest for molecular imaging and radiotherapy of prostate cancer.

Results

Preliminary Trial of Celluspots Array

To test the methodology, identify amino acid binding preferences of $[^{99m}Tc][Tc(CO)_3]^+$, and identify principles on which to base the design of a bespoke array to evaluate His-tag sequence variants, an array named STKS-1, originally designed to screen for serine/threonine kinase substrate activity and not for $[^{99m}Tc][Tc(CO)_3]^+$ binding, was used.[18,19] Its peptide sequences are shown in SI Table S2. It was radiolabeled with $[^{99m}Tc][Tc(CO)_3]^+$ and autoradiographed. Exemplar images (SI Figure S1) demonstrated sufficient resolution to measure the relative radioactivity of each spot. Some sequences stand out as having both higher labeling efficiency than others and higher stability after washing. Peptide-free control

Europe PMC Funders Author Manuscripts

Europe PMC Funders Author Manuscripts

spots showed no binding of radioactivity. When the array was incubated with [^{99m}Tc][TcO_4]$^-$, no spots showed significant radiolabeling.

Although the STKS-1 array contained no polyhistidine sequences, 68 sequences contained a single His and 16 had two or more, enabling several initial general observations to emerge by correlating radioactivity (DLU) with peptide sequence. All 300 sequences without histidine showed very low labeling efficiency, comparable to peptide-free control spots, even where cysteine (previously shown to enhance labeling of His-tagged proteins[13–15]) was present. Only peptides containing one or more His residues showed enhanced labeling (Figure 1A). A small number of the His-containing sequences did not show enhanced labeling compared to the His-free sequences. Thus, the presence of histidine is a necessary but not sufficient condition for labeling efficiency above that of controls. Surprisingly, the His-containing sequences with highest labeling efficiency had a calculated pI above 10 (Figure 1B). However, the combined presence of both a His residue and high pI did not guarantee high labeling efficiency. These features were among factors to be investigated in designing a new bespoke array focusing on the optimization of His-tag design for radiolabeling.

Design of Bespoke His-Tag Celluspots Array

A range of His-tag designs based on results from the STKS-1 array were incorporated into a bespoke array, spatially grouped according to features addressing specific questions about the number and arrangement of His residues and the effects of different accompanying amino acids. Sequences are listed in SI Tables S3 and S4 along with a description of the rationale for sequence design and grouping. Controls included a blank spot (controlling for radioactivity binding to the cellulose substrate), spots without a peptide but including the 3,6-dioxa-octanoic acid linker (controlling for binding to the linker), two non-His containing peptides with random amino acid combinations (to confirm that His residues are required for radiolabeling), the 4 sequences with the highest radiochemical yield from the trial STKS-1 Celluspots array (providing a quantitative link between the two arrays), and two published sequences for radiolabeling an affibody with [^{99m}Tc][$Tc(CO)_3$]$^+$ (to compare with effective published[20–24] sequences). Labeling and imaging the arrays with [^{99m}Tc][Tc-$(CO)_3$]$^+$ in PBS produced reproducible images exemplified by Figure 2; more comprehensive images are shown in SI Figure S2, along with a graph showing radiolabeling efficiency of every peptide in the array, color-coded according to groups (Figure S3). Despite almost all of the sequences (except controls) containing multiple His residues, some spots were labeled much more efficiently than others. While the labeling efficiency of all spots continued to increase between 15 and 120 min (SI Figures S2 and S4), all the main trends in labeling efficiency were amply evident by 15 min.

Correlation of Labeling Efficiency on Celluspots Array and in Solution

Before analyzing and interpreting data embodied in the images, the validity of this solid-phase method as a predictor of radiolabeling behavior in solution was tested by synthesizing ten peptides selected from the bespoke array, with a wide range of labeling efficiencies, and measuring their [^{99m}Tc][$Tc(CO)_3$]$^+$ labeling efficiency in PBS over time by ITLC-SA (see SI Figure S5 for exemplar chromatograms). Figure 3 shows that the solution labeling

efficiency (%) and the relative labeling efficiency in the array (DLU) were highly correlated with R^2 = 0.91, 0.93, 0.93, and 0.90 at 15, 30, 60, and 120 min, respectively.

Effect of Number and Arrangement of His Residues

Figure 4 shows the general trend that sequences with no His residues failed to label, and labeling efficiency broadly increased with number of His residues (up to 6). This should be interpreted cautiously because high pI significantly boosts labeling efficiency, and sequences with only four His residues (yellow in Figure 4A) were unrepresented in the pI > 8.5 group. Figure 4 also shows the relationship between labeling efficiency and pI separately for each group of arrangements of His-residues (excluding HHHH for reasons noted above). Despite interference from pI and other features, Figure 4B shows that HHHHHH sequences label more efficiently than HXHXHX residues (where X is a nonhistidine residue), which in turn are better than HXHX and HXXH. There is overlap, however, mainly due to variation in pI.

Effect of pI

The summary plot in SI Figure S3 draws attention immediately to the prominence of the high pI group of peptides (containing positively charged amino acids alongside the His tag) among the most efficiently labeled sequences. This was the case for all groups of His arrangements (SI Figure S6), reaching DLU values almost 10-fold higher than the bulk of the His-tag sequences. The high pI group had at least 2 and up to 5 Lys or Arg residues, and showed labeling enhancements that were much more pronounced than that caused by including Cys. Some other groups of sequences also had a few members with elevated labeling efficiencies; on close inspection, these turned out also to contain positively charged amino acids. Figure 5A shows that, of the 78 sequences containing 2–4 Glu or Asp (negatively charged) residues (average pl 5.4), all had low labeling efficiencies, while of the 49 sequences containing 2–4 Lys or Arg residues (average pl 11.1), all had significantly higher labeling efficiencies ($p < 0.005$), and there was no overlap in the labeling efficiencies of the two groups. The design of the array allowed comparison of pairs of His tag sequences that were identical except for a single “point mutation”, in which one residue was varied. These pairs again highlighted labeling enhancement caused by positively charged amino acids, and demonstrated a detrimental effect of negatively charged amino acids (Figure 5B). In six series of such point-mutated sequences, replacing either the positively or negatively charged amino acid with an uncharged amino acid led to an intermediate labeling efficiency (SI Figure S7). Although sequences with 2–5 positively charged residues gave the highest labeling efficiencies, even a single positively charged residue consistently and significantly enhanced labeling efficiency. The effect of pI within the different types of His tag is further highlighted in SI Figure S6. Further analysis, grouping sequences according to the number of positively charged residues alongside the His-tag, showed that a second Arg significantly increases labeling efficiency, while a third gave an enhancement of borderline significance and a fourth gave no further enhancement (SI Figure S8). A similar effect was observed for Lys, except that a third Lys significantly enhanced labeling efficiency compared to the second (SI Figure S9). Arg residues increased labeling efficiency more effectively than Lys (SI Figure S10). Among His tags containing multiple Arg residues, those with six consecutive His residues showed higher labeling efficiency than sequences in which the Arg residues interrupted the His sequences (e.g., RHRHR, RHRHRHR, RHRRHR; SI Figure

Europe PMC Funders Author Manuscripts
Europe PMC Funders Author Manuscripts

S11). However, this observation should be interpreted cautiously, since several potential alternative His tag arrangements were missing from the array; it is unclear whether the smaller number of His residues or the location of the Arg residues caused the poor labeling of these interrupted His-tags.

Influence of Cysteine and Methionine

Because of previous reports that Cys close to the His-tag could enhance labeling efficiency,[13–15] considerable space on the array was allocated to investigating this effect. A positive influence, although much less striking than that of positively charged amino acids, was found. Among the ten sequences (SI Table S5) with best labeling efficiency, seven included Cys, while all had high pI and multiple Arg residues. For each of these seven Cys-containing sequences, direct comparison of $[^{99m}Tc][Tc\text{-}(CO)_3]^+$ labeling was possible with a partner sequence that was identical except for the omission or substitution of the Cys residue (Figure 6a). In all except GGRHHHRHHHRGGC, the presence of Cys enhanced labeling efficiency, without clear preference for the location of the Cys. Interestingly, despite the trend of increased labeling efficiency with increased numbers of His residues, one peptide with only 3 His residues featured in the top 10, probably because it has both abundant (five) Arg residues and a Cys residue.

To determine whether the labeling enhancement due to Cys could be similarly achieved by Met instead (since both thiolates and thioethers are typically strong ligands for low oxidation state technetium and rhenium), 12 pairs of sequences were included that were identical except that Cys was replaced by Met. For 4 of these pairs, a third sequence was present in the array that was identical with the other 2 except that neither Cys nor Met was present. Figure 6B shows that in all pairs there was no significant difference in labeling efficiency between the Cys and the Met analogues, while all sequences with neither labeled significantly less efficiently than their Cys- and Met-containing partners. None of these sequences had high pI and so were not among the most efficiently labeled in the array.

Influence of pH and Buffer Composition on Labeling

To compare labeling in different buffers, the array was incubated with the same $[^{99m}Tc][Tc(CO)_3]^+$ activity and for the same time in PBS buffer at pH 7.4, citrate buffer at pH 5.5, and tris-HCl buffer at pH 8.8 and pH 7.4. In the citrate and tris-HCl buffers, although His-containing peptides showed labeling efficiency higher than control (“no peptide” or “His-free” peptide) spots, labeling was poor compared to that in PBS even after 120 min. Moreover, the marked enhancements seen in PBS with positively charged sequences were not apparent. The difference in pH may contribute to, but cannot fully explain, these findings; one of the Tris-HCl buffers had a pH of 7.4 (similar to PBS), and although the labeling efficiencies were about 2-fold higher than in Tris-HCl at pH 8.8, they were not comparable to those in PBS. In addition, in the case of citrate buffer, washing the labeled arrays with histidine solution removed a large fraction of the radioactivity; this did not occur after labeling in PBS or tris-HCl (SI Figures S12–S16).

Europe PMC Funders Author Manuscripts
Europe PMC Funders Author Manuscripts

Europe PMC Funders Author Manuscripts

Europe PMC Funders Author Manuscripts

Stability of Radiolabeled Peptides

Arrays that had been $[^{99m}Tc][Tc(CO)_3]^+$-labeled in PBS were incubated in fresh PBS pH 7.4 or in human serum (as an initial guide to likely *in vivo* stability) for up to 24 h and imaged periodically. There was no significant loss of radioactivity from His-tagged sequences on incubation with PBS (SI Figures S17 and S18) or serum (Figure 7; additional data shown in SI Figures S19 and S20) even after 24 h. Only the control spots, containing His-free peptides or no peptide, showed significant loss, and this loss was faster in serum than in PBS, suggesting that transchelation from His-free sequences to serum constituents (such as protein His residues) occurs. Similarly, radiolabeled His-tagged sequences quantitatively retained radiolabel when challenged with a large excess of histidine or cysteine (SI Figures S21 and S22).

Radiolabeling with Rhenium-188

To determine the extent to which the potentially therapeutic analogues $[^{186/188}Re(CO)3]^+$ mimic the labeling efficiency and sequence selectivity of $[^{99m}Tc][Tc(CO)_3]^+$, the His-tagged peptide array was incubated in PBS with $[^{188}Re(CO)_3]^+$ and imaged as before. As expected, because of the high energy of the β-particles, the resolution of the electronic autoradiographs was poor compared to that of the ^{99m}Tc images (which arise mainly from very low energy Auger electrons). Nevertheless, visual correspondence between the ^{99m}Tc and ^{188}Re images was clear (SI Figure S23), showing that the sequence selectivity was the same for both radiometals. Indeed, the sequence with highest labeling efficiency was CLRRRLAHHHHHH for both ^{99m}Tc and ^{188}Re (SI Figure S24). For the weakest-binding sequences, binding of ^{188}Re was lower than that of ^{99m}Tc (that is, selectivity for the better His-tags was somewhat greater for ^{188}Re). Radiochemical stability in serum and competing buffers was also similar for both ^{99m}Tc- and ^{188}Re-labeled peptides (SI Figure S25).

Electrophoresis of "$[^{99m}Tc][Tc(CO)_3]^+$"

To determine the mean charge associated with the putative $[^{99m}Tc][Tc\text{-}(CO)_3]^+$ synthetic intermediate, $[^{99m}Tc][Tc(CO)_3]^+$ was compared to $[^{99m}Tc][TcO_4]^-$ (as a readily available standard ^{99m}Tc-monoanion) and $[^{99m}Tc]$-sestamibi (as a readily available standard known ^{99m}Tc-cation) by electrophoresis in PBS (pH 7.4, see Figure 8), tris-HCl (pH 7.4 and 8.8) and citrate buffer pH 5.1 (SI Figure S26), followed by phosphor imaging. $[^{99m}Tc][TcO_4]^-$ and $[^{99m}Tc]$-sestamibi behaved as expected in all buffers, migrating toward the anode and cathode, respectively. $[^{99m}Tc][Tc(CO)_3]^+$, however, migrated toward the cathode in tris-HCl buffer at both pH 7.4 and pH 8.8, but toward the anode in both PBS and citrate buffer, contrary to its commonly supposed identity as $[^{99m}Tc][Tc\text{-}(CO)3(H2O)3]^+$.

^{31}P NMR of $[Re(CO)_3(H_2O)_3]^+$

^{31}P NMR spectra of 100 mM PBS were acquired, giving a single signal with $\delta = 2.0$, and again after addition of $[Re(CO)_3(H_2O)_3]Br$ at concentrations of 0.5, 1.0, 2.0, and 5.0 mM, equilibrating at room temperature for 30 min upon each addition. Up to 7 significant new resonances appeared downfield of the phosphate singlet, indicating the presence of new phosphate-containing species (SI Figure S27). The integrated signal intensity of the new species totalled about 5% of that of the original phosphate signal, suggesting an average 1:1

Europe PMC Funders Author Manuscripts

Europe PMC Funders Author Manuscripts

ratio of phosphate to rhenium in the new species even in the presence of a large excess (at least 20-fold) of phosphate. No further change occurred after heating to 37 °C. The results suggest that phosphate displaces coordinated water and coordinates to $[Re(CO)_3]^+$ and, by analogy, to $[Tc(CO)_3]^+$, thus converting the cationic complex to an anionic one, consistent with the electrophoresis of $[^{99m}Tc][Tc(CO)_3]^+$ in phosphate buffer.

Proteins Incorporating an Optimal His-Tag Sequence

A trial peptide sequence ALRRRLAHHHHHH, which was the most efficiently radiolabeled sequence (in PBS at pH 7.4) and included three Arg residues, was selected from the His-tag array and designated “JWT”. A single chain antibody fragment (scFv) J591scFvJWT, one of several fragments[25,26] derived from the J591 antibody[27–30] directed against the prostate specific membrane antigen (PSMA), was engineered to include a C-terminal His-tag that includes the JWT sequence. The labeling properties of this protein were compared with four similar scFv antibody fragments containing His-tags that were not optimized: J591scFv (the “parent” J591scFv, identical with J591scFvJWT except that its C-terminal His-tag sequence is KRAAALEHHHHHH which contains no Arg residues); huJ591scFv (a humanized version of the J591scFv which contains the Arg-free C-terminal His tag sequence IKAAALEHHHHHH); 6C7.1scFv, a single chain antibody directed against mouse vascular cell adhesion molecular 1 (VCAM-1)[31] and incorporating the C-terminal His-tag sequence PTAAALEHHHHHH; and 6C7.1scFvCys (identical with 6C7.1scFv except that the His-tag has an additional Cys residue at the C-terminus, TAAALEHHHHH-HC). Production and characterization of these proteins are described in SI Figures S28–S30.

$[^{99m}Tc][Tc(CO)_3]^+$-labeling efficiencies of the proteins in PBS, pH 7.4, at 37 °C for up to 120 min, at a range of protein concentrations from 0.9 to 28 μM are shown in Figure 9 and a wider range is shown in SI Figure S31. Labeling of the JWT-tagged protein was dramatically more efficient than that of the other four. It was the only protein to reach a labeling efficiency of >95% within 30 min at any concentration or at a concentration as low as 7 μM at any time up to 120 min (SI Table S6). No other proteins reached a labeling efficiency of 95% at concentrations below 28 μM, or in less than 90 min. J591scFvJWT was also radiolabeled at 25 °C with only marginal reduction in labeling efficiency at any time point compared to 37 °C (see SI Figure S32).

Biological Behavior of $[^{99m}Tc(CO)_3]^+$-J591scFvJWT

To determine whether the JWT tag adversely affected the molecular imaging utility of the protein, $[^{99m}Tc][Tc(CO)_3]^+$-J591scFvJWT was subjected to measurement of serum stability (by ITLC-SA and SDS-PAGE), binding to the PSMA target *in vitro*, and in *vivo* biodistribution and SPECT imaging. Upon incubation of $[^{99m}Tc][Tc(CO)_3]^+$-J591scFvJWT in human serum at 37 °C for 4 h, no non-protein-bound ^{99m}Tc was detected by ITLC-SA (i.e., radiochemical purity was >98.9% at all time points); SDS-PAGE followed by phosphor imaging revealed only a single radioactive band corresponding to the molecular weight of J591scFvJWT (ca. 28 kDa), whereas $[^{99m}Tc][Tc(CO)3]^+$ in human serum gave rise to a single radioactive band with molecular weight >50 kDa (SI Figure S33). Serum stability of the other four labeled proteins by these methods showed similar results (data not shown).

Europe PMC Funders Author Manuscripts

The PSMA-binding affinity of J591scFvJWT was measured using PSMA-expressing and -nonexpressing prostate cancer cells (DU145-PSMA and DU145, respectively[26]) using increasing concentrations (0.06–3559 nM) of J591scFvJWT as a competitive blocker and trace levels (1 nM) of $[^{99m}Tc][Tc(CO)_3]^+$-J591scFvJWT as a probe. A parallel experiment was performed similarly with huJ591scFv and $[^{99m}Tc][Tc(CO)_3]^+$-huJ591scFv for comparison. Both radiolabeled proteins showed specific, inhibitable binding to DU145-PSMA but not to DU145 cells, with IC_{50} values of 3.2 nM for J591scFvJWT and 4.0 nM for J591scFv (SI Figure S34). Thus, both labeled His-tagged proteins bound specifically to PSMA, and the affinities of both unlabeled proteins for PSMA were similar. However, the presence of the JWT tag, with its three Arg residues, was associated with a significantly higher level of nonspecific binding to both cell lines.

Confirmation of the stability and target-binding function of $[^{99m}Tc][Tc(CO)_3]^+$-J591scFvJWT in *vitro* justified its in vivo evaluation for imaging PSMA-positive tumors. Mice bearing DU145 or DU145-PSMA human prostate cancer-derived tumor were SPECT-CT-scanned 75–100 min post-injection of $[^{99m}Tc][Tc(CO)_3]^+$-J591scFvJWT or $[^{99m}Tc][Tc(CO)_3]^+$-J591scFv. As well as a distribution typical of scFv proteins in normal tissues (rapid clearance from blood, moderate liver uptake, and high kidney uptake), both tracers showed elevated uptake in PSMA-positive tumors, but not in PSMA-negative tumors, compared to other tissues (Figure 10). Similarly, *ex vivo* biodistribution data from animals ($n = 4$) culled 90 min post-injection showed that both proteins were taken up in DU145-PSMA but not DU145 tumors, and showed similar high kidney uptake (>100%ID/g); however, J591scFvJWT had approximately 3-fold higher liver uptake (30%ID/g), 4-fold lower retention in blood, 3-fold lower uptake in PSMA-positive tumor, and a higher tumor-to-blood ratio, compared to J591scFv (Figure 10).

Discussion

Despite fragmentary investigation of the structures of protein adducts with $[Re(CO)_3]^+$ [15,32–35], little is known about the preferred amino acids or the coordination chemistry of the interactions. After evaluating the principle and methodology of use of a solid-phase peptide array for optimizing amino acid sequences for radiolabeling, a bespoke His-tag array was designed to optimize a His-tag-based sequence for efficient labeling with $[^{99m}Tc][Tc(CO)_3]^+$, addressing a set of questions arising from both previously published data and results from the STKS-1 array described above: (1) Building on the observation (from STKS-1 array experiments) that a His residue is necessary but not sufficient for even moderately efficient labeling, what is the optimum number and arrangement of His residues, including interruption with other amino acids and embedding within a sequence[16,21,24] (rather than at the terminus)? (2) Building on the observation (from STKS-1 array) of the enhancing effect of high pI, what is the effect of positively charged, negatively charged, and uncharged amino acids near to the His-tag? (3) Building on published observations, how does the presence of one or more Cys residues, at different positions relative to the His-tag, affect labeling, compared to the same sequence without Cys?[13,15] (4) Building on published indications that thioethers are potent ligands for $[M(CO)_3]^+$[36–41] and other low oxidation state rhenium and technetium complexes,[42–44] can Met residues (which may be preferable to

Europe PMC Funders Author Manuscripts

Europe PMC Funders Author Manuscripts

Cys because they avoid problems of protein folding related to disulfide bond formation) produce a similar labeling enhancement to Cys?

Radiolabeling the bespoke His-tag array showed a wide and reproducible variation in labeling efficiency of different sequences. The synthesis and radiolabeling efficiency of ten selected peptides in solution showed strong correlation with relative solid-phase labeling efficiency, and so we can be confident that the labeling behavior observed for the array would be highly predictive of solution phase labeling and helpful in optimizing a His-tag design for radiolabeling.

Analysis of the labeling efficiency data from the array revealed several useful design parameters that contribute to efficient labeling with $[^{99m}Tc][Tc(CO)_3]^+$. First, several sequential or nearly sequential His residues are better than one, with incremental improvements observed as the number of His residues was increased to six; nine of the best ten sequences contained six His residues. Second, incorporation of positively charged residues (Arg, Lys) adjacent to or within the His tag sequence, associated with a high pI, dramatically improved labeling efficiency; conversely, negatively charged residues were detrimental to labeling, while uncharged residues are comparatively neutral in their effect. The range of labeling efficiency values among the various His-tag designs was striking: His-tags with adjacent positively charged residues could be labeled as much as 40 times more efficiently than those with adjacent negatively charged residues. This is a surprising observation, suggesting that the putative positive charge of the labeling synthon $[M(CO)_3(H_2O)_3]^+$ warranted further investigation, discussed below. It is also apparent that interrupting hexahistidine sequences with glutamate (as in the “HEHEHE” tags), a modification introduced to improve biodistribution of the labeled protein,[20–24] is significantly detrimental to labeling efficiency. Third, the previously observed[13–15] advantage of incorporating cysteine close to the His-tag was confirmed, but its enhancing effect was minor compared to the effect of positively charged residues. Fourth, methionine could also enhance labeling in a similar manner to cysteine; data supporting this observation were less comprehensive than those supporting the more dramatic effects mentioned above, because the array included fewer examples of Met-containing sequences. Nevertheless, further investigation of Met incorporation is warranted. The overall outcome of this optimization was an increased labeling efficiency of around an order of magnitude compared to the best “conventional” His tags (see SI Figure S35) already reported as having good labeling properties.[13–16,21,24]

The similarity of the labeling pattern of the array when exposed to either $[^{99m}Tc][Tc(CO)_3]^+$ or $[^{188}Re(CO)_3]^+$ indicates that the same trends and preferences apply whether technetium or rhenium is used. This is important for confidence in the use of ^{99m}Tc (SPECT imaging) and ^{188}Re (radionuclide therapy) as an analogous “theranostic pair”.[6,45]

At the outset, it was intuitively expected that negatively charged residues close to the His-tag would have a positive kinetic effect on labeling due to favorable electrostatic interaction with the positively charged incoming [M-(CO)3(H2O)3] $^+$ ion. It was therefore surprising to observe instead that aspartate and glutamate were detrimental to labeling compared to uncharged residues, while radiolabeling was significantly enhanced by proximity of

Europe PMC Funders Author Manuscripts

Europe PMC Funders Author Manuscripts

positively charged residues. This led us to question the assumption that [M(CO)3(H2O)3] $^{+}$ is the major tricarbonyl species present in the buffers used. The electrophoresis experiments showed that while the [^{99m}Tc(CO)$_3$]$^+$-containing species is indeed cationic in tris-HCl (pH 7.4 and 8.8), in both PBS (pH 7.4) and citrate buffer (pH 5.1) it is anionic. One may envisage the negative charge resulting from either ionization of two of the coordinated water molecules, or substitution of one or more coordinated water molecules by the buffer anion, phosphate or citrate, or possibly chloride ions. Some possible structures are shown in Figure 11. Ionization of coordinated water in [M(CO)$_3$(H$_2$O)$_3$]$^+$, under appropriate pH conditions, is known[46] but may be discounted as the cause in these experiments, because the complex remains cationic in tris-HCl at pH 7.4 and even at pH 8.8. Coordination of chloride may also be discounted for similar reasons. Tricine is known to react with [Re(CO)$_3$(H$_2$O)$_3$]$^+$, albeit under refluxing conditions, displacing water and coordinating as a tridentate ligand (alkoxide, alcohol, and amine, as determined by X-ray crystallography),[47] to give an uncharged complex; but characterization of the complex by NMR was precluded by its dissociation, hence the complex has a low formation constant. Coordination of phosphonate groups of 1,2-bisphosphonate to [Re(CO)$_3$]$^+$ has been observed,[48] but we have found no reports of phosphate or citrate complexes with [M(CO)$_3$]$^+$. ^{31}P NMR studies of a 5:1 excess of phosphate over [Re(CO)$_3$(H$_2$O)$_3$]$^+$ showed a 20% reduction in phosphate signal, with the deficit made up by several new peaks. This stoichiometry is consistent with an average 1:1 complex formation between phosphate and metal center (e.g., Figure 11B,C), which explains the anionic behavior on electrophoresis. Thus, an electrostatic effect could be invoked whereby the anionic complex has a locally enhanced concentration near the His-tag by virtue of ion pairing with the neighboring cationic residues. However, a similar enhancement is not observed in citrate buffer, in which the radiometal complex is also anionic (shown by electrophoresis); moreover, there was no enhanced labeling of sequences with negatively charged residues in Tris-HCl buffer. These observations suggests that some additional, phosphate-specific effect occurs; since phosphate is known to interact strongly with arginine residues through a combination of hydrogen bonding and ion pairing, forming a “salt bridge”,[49,50] we hypothesize that such an interaction (Figure 11G), in which phosphate serves as a bridge between cationic Arg (or Lys) and [M(CO)$_3$]$^+$, could have the effect of increasing the rate of complexation with His residues by increasing the local concentration of the [M-(CO)$_3$]$^+$ moiety. Since histidine side-chains are also somewhat basic and the histidine sequence itself will carry some positive charge at the labeling pH, a similar electrostatic interaction may be involved in labeling even in the absence of Arg or Lys residues, albeit weaker, because the strongly hydrogen-bonded salt bridges of the type shown in Figure 11G cannot be involved. This might explain the relatively poor labeling of all sequences when phosphate buffer was not used. Thus, as well as the neighboring amino acid residues, the choice of buffer plays a major role in the efficiency of radiolabeling, and further optimization should examine both.

The true test of the optimized His-tag is to incorporate it into a protein and compare its labeling with that of analogous proteins that have “conventional” His-tags. The example shown here, in which the best-performing sequence from the bespoke array, named “JWT”, was evaluated, showed significant enhancement of labeling efficiency compared to the non-optimized controls, whether the criterion was the lowest concentration of protein, or the

Europe PMC Funders Author Manuscripts

Europe PMC Funders Author Manuscripts

shortest time, needed to attain 95% labeling efficiency at a given temperature. The 95% criterion was chosen, because this is a typical radiochemical purity level at which radiopharmaceuticals are deemed suitable for clinical use. Although this single example is not enough to confirm the generalization that incorporation of the JWT-tag, and others like it, confer dramatically enhanced labeling efficiency on any protein, it is gratifying that the effect is so striking.

It was important to check that, once labeled, the biological properties of the protein are not adversely affected compared to the same proteins with conventional His-tags. Accordingly, we checked stability of the radiolabeled protein in serum, affinity for the PSMA-expressing target cells in *vitro*, and in vivo biodistribution, tumor targeting, and imaging capability. None of these were adversely affected, although there was an undesirable increase in nonspecific binding to non-PSMA-expressing cells in *vitro*. We therefore found no reason to suspect that the enhancement of labeling efficiency would in general come at the cost of systematically inferior *in vivo* targeting properties. Some studies of the effect of varying the His-tag sequence on biodistribution have been performed,[20,23,24,51–53] but they have not identified very significant effects on tumor targeting, liver uptake, or kidney uptake. Moreover, they typically involved only a small number of related proteins; consequently, they produce no generalizable conclusions about choosing sequences for optimal biodistribution. However, unusually abundant arginine and cysteine residues in proteins can have dominant effects on protein folding by virtue of their ability to form strong hydrogen bonds and salt bridges (Arg) or disulfide bonds (Cys), so it is reassuring to note that the beneficial effects of Arg residues in the tag can be replicated by Lys, and those of Cys by Met; proteins incorporating some of the other efficiently performing sequences from the array, containing Lys and Met, should also therefore be evaluated.

Conclusion

We have shown that labeling of His-tags in proteins with $[^{99m}Tc][Tc(CO)_3]^+$ and $[^{188}Re(CO)_3]^+$ can be dramatically enhanced (more than 40-fold) by optimizing both the design of the His-tag (to incorporate neighboring Arg or Lys residues and remove negatively charged residues, with a smaller additional effect from Cys and Met) and the choice of buffer (phosphate was critical in achieving these enhancements). As a result, it is possible to radiolabel proteins incorporating such tags quickly in a single step, under mild conditions of pH and temperature, without the need for post-labeling purification, to give radiochemically pure products with much higher molar activity than conventionally His-tagged proteins. The simplicity and convenience of production afforded by this design enhancement will make protein-based radiopharmaceuticals for molecular imaging and therapy based on generator-produced ^{99m}Tc and ^{188}Re more attractive and widely available for clinical use, extending their benefits to more hospitals and patients.

Experimental Procedures

Solvents and chemicals were purchased from Sigma-Aldrich unless otherwise indicated.

Europe PMC Funders Author Manuscripts

Europe PMC Funders Author Manuscripts

Synthesis of $[^{99m}Tc][Tc(CO)_3(H_2O)_3]^+$

$[^{99m}Tc][TcO_4]^-$ (2200–2500 MBq in 400 μL saline), eluted from a Drytec generator (GE Healthcare, Amersham, UK) was added to an Isolink kit (donated by Covidien, Petten, The Netherlands) following the manufacturer's instructions. Quality control was performed by thin layer chromatography (TLC) using silica gel $60F_{254}$ TLC plates (Merck Millipore, Darmstadt, Germany) with a mobile phase of 1% HCl in methanol (in which $[^{99m}Tc][TcO_4]^-$ has Rf = 0.9, ^{99m}Tc colloids have Rf = 0, and $[^{99m}Tc][Tc(CO)_3]^+$ has Rf = 0.2–0.8 (SI Figure S1). Chromatograms were analyzed with a gamma TLC plate scanner (Lablogic, UK). In all experiments, the product $[^{99m}Tc][Tc(CO)_3]^+$ was >95% radiochemically pure with <<1% contamination with ^{99m}Tc-colloid (see SI Figure S36).

Synthesis of $[^{188}Re(CO)_3(H_2O)_3]^+$

A previously published method was used,[54] starting from $[^{188}ReO_4]^-$ (1 mL, 38 MBq) eluted with physiological saline from a 7.4 GBq $^{188}W/^{188}Re$ generator (ITG, Garching GmbH, Germany). The product was analyzed by TLC as described above. Rf values were similar to those of the ^{99m}Tc analogues. Radiochemical purity was typically 82%. Purification was performed using a two-column system as previously described[54] giving a final radiochemical yield of 61% with radiochemical purity >99%.

Synthesis of $[Re(CO)_3(H_2O)_3]Br$

This complex was prepared as previously reported[36] from $[Re(CO)_5Br]$ (Strem Chemicals Inc., Cambridge, UK).

Peptide Molecular Weight and pI

The molecular weight and theoretical pI of all peptide sequences were calculated using compute pI/Mw by ExPASy Bioinformatics Resource Portal and UniProt Knowledgebase (Swiss Prot or TrEMBL) entries or user-entered sequences.

Celluspots Array Labeling and Analysis

The Cellus-pots array (STKS-1, donated by Intavis Bioanalytical Instruments AG, Koeln, Germany; for details of sequences, see SI Table S2) was used for an initial trial and method development. A bespoke His-tag array was then designed and purchased from the same source. Details of the array, including the rationale for sequence selection, are given in SI Tables S3 and S4. The array was fully immersed in a 50 mL Falcon tube containing 50 mL of phosphate buffered saline (PBS) at pH 7.4 containing $[^{99m}Tc][Tc(CO)_3(H_2O)_3]^+$ (8 MBq), $[^{188}Re(CO)_3(H_2O)_3]^+$ (2 MBq), or $[^{99m}Tc][TcO_4]^-$ (control) and incubated at 37 °C for 15 min with gentle shaking. The array was then washed in fresh PBS for 3 s, gently blotted, exposed to the phosphor film for 5 min (^{99m}Tc) or 4 min (^{188}Re) and immediately reimmersed in the $[^{99m}Tc][Tc\text{-}(CO)_3]^+$ or $[^{188}Re(CO)_3(H_2O)_3]^+$ solution for further incubation/washing/imaging cycles to give total times of 30, 60, 90, and 120 min. The phosphor films were imaged with a Cyclone phosphor imager (PerkinElmer). Images were processed using the Opti-quant program (PerkinElmer) with each spot in a square grid element. The intensity of each spot was recorded as DLU (digital light unit), an arbitrary unit proportional to its radioactivity. The experiment was repeated for three slides, each with

Europe PMC Funders Author Manuscripts

Europe PMC Funders Author Manuscripts

two duplicate arrays (overall $n = 6$). Two-tailed t tests were used to evaluate the significance of differences in radiochemical yield between selected pairs of peptides. The same labeling procedure was performed with citrate buffer (pH 5.5), Tris-HCl buffer (pH 8.8) and Tris-HCl buffer (pH 7.4) in place of PBS.

To determine the stability of the radiolabeled arrays, after a single radiolabeling incubation of 120 min, washing and phosphor imaging as above, the labeled arrays were immediately immersed in 50 mL of human male AB plasma (Sigma-Aldrich, UK, diluted 1:1 with saline), fresh PBS buffer (pH 7.4), 5 mM cysteine in PBS (pH 7.4), or 5 mM histidine in PBS (pH 7.4), for 60 min at 37 °C with gentle shaking, washed in PBS, blotted and phosphor imaged as before, and returned to their incubation solutions for a further 60 min. The array was imaged again after a further 22 h (for PBS and serum) or 1 h (for cysteine and histidine). At the 2 and 24 h time points, the phosphor film exposure times were extended to 10 and 30 min, respectively, (^{99m}Tc) or 15 and 30 min (^{188}Re) to allow for radioactive decay. The DLU of each spot at each washing time was expressed as a % of that of the corresponding spot after the initial 120 min labeling period, corrected for the increased exposure time and for radioactive decay (one slide, $n = 2$).

Solution Phase Peptide Labeling

Ten exemplar peptides with sequences (SI Table S7) selected from the array to give a broad range of labeling efficiencies were synthesized using standard solid-phase methods, and analyzed by electrospray mass spectrometry, as detailed in SI Table S8. A 250 μM solution of each in 10% acetonitrile in PBS, pH 7.4, was prepared and used to prepare a 5-fold dilution series with concentrations of 250, 50, 10, and 2 μM. To 20 μL of each solution, $[^{99m}Tc][Tc(CO)_3]^+$ (20 μL, 40 MBq) was added followed by incubation at 37 °C. The solutions were sampled at 5, 15, 30, 60, and 90 min to determine radiochemical yield using ITLC-SA strips, developed (after air-drying the spots) with 0.1 M citrate buffer (pH 5) to separate labeled peptides (Rf = 0) from unbound $[^{99m}Tc][Tc(CO)_3]^+$ and $[^{99m}Tc]$-$[TcO_4]^-$ (Rf = 1).

Electrophoresis

Electrophoresis of $[^{99m}Tc][TcO_4]^-$ (monoanion standard), [^{99m}Tc]-Sestamibi (monocation standard, prepared from SestaMIBI Mallinckrodt kits according to manufacturer's instructions), and $[^{99m}Tc][Tc(CO)_3]^+$ was performed using a 30 × 32 cm^2 system (Scie-Plas) with cellulose acetate strips (Sigma-Aldrich, UK) spotted equidistant from anode and cathode with 0.5 μL of 40–50 MBq/mL samples. The chamber was filled with 0.01 M PBS, 0.05 M Tris-HCl (pH 8.8), 0.05 M Tris-HCl (pH 7.4), or 0.1 M citrate (pH 5.1) buffer. A constant current of 4 mA was applied for 1 or 2 h. A radioactive marker was applied to mark the original spot position and the anode/cathode orientation, and the strips were exposed to phosphor film for 2–3 min as described above. Experiments were performed in triplicate.

^{31}P NMR Spectroscopy

$[Re(CO)_3(H_2O)_3]Br$ was dissolved in 0.1 M phosphate buffer (pH 7.4) to give concentrations of 0.5, 1.0, 2.0, and 5.0 mM. 10% D_2O was added to each to provide a deuterium reference. ^{31}P NMR spectra (512 scans) were acquired of these solutions, and of

identically prepared phosphate buffer without [Re-$(CO)_3(H_2O)_3$]Br, immediately at room temperature and after heating the samples for 30 min at 37 °C, using a Bruker NMR spectrometer at 161.7 MHz with ^{1}H decoupling. Data were processed using Bruker's Topspin 5.1 software.

Model Protein Labeling

The design, production, purification, characterization, and [^{99m}Tc][$Tc(CO)_3]^+$ radiolabeling of the model His-tagged scFv proteins and their key properties (Table S9) are described in Supporting Information. Concentrations of protein stock solutions in PBS, pH 7.4 were: 42 μM, 1.2 mg/mL for J591scFvJWT, J591scFv, and huJ591scFv; 21 μM, 0.6 mg/mL for 6C7.1scFv; 10.5 μM and 0.3 mg/mL for 6C7.1-CscFvs Protein concentrations were determined by UV absorption at 280 nm using a Nanodrop spectrophotometer. 2-fold dilution series were prepared with six protein concentrations: 42 μM, 21 μM, 10.5 μM, 5.25 μM, 2.625 μM, and 1.312 μM. Because of restricted quantity available, the highest concentration of 6C7.1scFv and the two highest concentrations of 6C7.1-CscFvs were missing from the series. To the scFv proteins (approximately 25 μL), 10 μL (approximately 50 MBq) of [^{99m}Tc][$Tc(CO)_3]^+$ was added to give 2 MBq/μg for the protein samples with the highest concentration (which contained a total of approximately 25 μg protein). The solutions were incubated at 37 °C, sampling at 15, 30, 60, 90, and 120 min for ITLC-SA analysis as described above for synthetic peptides. The strips were cut in half and each half counted in the gamma counter. Experiments were performed in duplicate. In addition, for J591scFvJWT (14.1 μM, 0.4 mg/mL) the [^{99m}Tc][$Tc(CO)_3]^+$ labeling was compared at 37 and 25 °C, and with 0.1 M citrate buffer (pH 5.5) in place of PBS.

Serum Stability of [^{99m}Tc][$Tc(CO)_3]^+$-J591scFvJWT

J591scFvJWT was radiolabeled with [^{99m}Tc][$Tc(CO)_3]^+$ as described above. Once the radiochemical yield had reached 95% as determined by ITLC-SA, the solution was incubated at 37 or 25 °C (for comparison) with an equal volume of fresh human serum isolated from human blood, sampling at 0, 15, 30, 60, 120, and 240 min for ITLC-SA analysis (as above, to detect any release of low-molecular-weight ^{99m}Tc). Additional samples obtained at the same time points were immediately frozen in liquid nitrogen and later analyzed by SDS-PAGE (12% NuPAGE, Invitrogen, to detect transfer of ^{99m}Tc to serum proteins). Gels were visualized by Coomassie blue staining and electronic autoradiography using a phosphor imager.

Target Binding of Labeled Proteins

A homologous cell binding competition was performed for the [^{99m}Tc][Tc-$(CO)_3]^+$-labeled J591scFvJWT, J591scFv, and huJ591scFv to assess binding to prostate cancer cell lines DU145 with (DU145-PSMA) and without (DU145) PSMA expression.[20] Cells (4×10^4/well) were seeded and grown overnight in a 96-well plate, then incubated with serial dilutions of J591scFvJWT (3559 nM to 0.06 nM) along with a constant concentration of [^{99m}Tc][$Tc(CO)_3]^+$-J591scFvJWT (1 nM) for 45 min at 4 °C, then washed three times with 100 μL cold PBS and lysed by treatment twice with 50 μL of 0.5 M NaOH. The combined NaOH extracts (cell-associated radioactivity) were counted using the gamma counter and data analyzed using GraphPad Prism with a "one site total binding" algorithm.

Europe PMC Funders Author Manuscripts
Europe PMC Funders Author Manuscripts

Europe PMC Funders Author Manuscripts

In Vivo PET and *Ex Vivo* Biodistribution

Animal studies were carried out in accordance with UK Research Councils' and Medical Research Charities' guidelines on Responsibility in the Use of Animals in Bioscience Research, under UK Home Office project and personal licenses. Male SCID beige mice aged 6 to 10 weeks (Charles River, Margate, UK) were used for all experiments. Cells ((3–4) × 10^6 DU145 or DU145-PSMA cells) were injected subcutaneously on the left flank in 50 μL RPMI 1640 medium, and animals were used for imaging or biodistribution studies after 4 weeks, when tumor diameter was approximately 5 mm. J591scFvJWT and J591scFv (52 μg each) were radiolabeled with $[^{99m}Tc][Tc(CO)_3]^+$ (1000 MBq) as described above, ensuring >95% labeling efficiency by ITLC-SA. The labeled proteins were diluted with saline to achieve a radioactive concentration of 0.375 MBq/μL. Mice (n = 4 for each group) were maintained under isoflurane anesthesia with respiration monitoring and injected via a tail vein with 30 MBq of the labeled protein in 80 μL PBS. Helical SPECT/CT images were acquired at 75–90 min postinjection, and then mice were immediately sacrificed. SPECT images were reconstructed with Hi-SPECT software (Bioscan, Washington, DC, USA). CT images were reconstructed using the SPECT/CT scanner-embedded software package. To quantify tumor and muscle uptake, tissues were identified by reference to CT images and regions of interest covering the entire organ/tumor were drawn in all slices. Time-activity curves were generated for tumors. Organs were harvested, briefly washed in PBS, blotted, and weighed. Activity in whole organs and tumors was measured by gamma counting.

Supplementary Material

Refer to Web version on PubMed Central for supplementary material.

Acknowledgments

This work was supported by the Biomedical Research Centre Award to Guy's & St Thomas' NHS Foundation Trust in partnership with King's College London and King's College Hospital NHS Foundation Trust; the Centre of Excellence in Medical Engineering funded by the Wellcome Trust and EPSRC under grant WT088641/Z/09/Z; the King's College London and UCL Comprehensive Cancer Imaging Centre funded by the CRUK and EPSRC in association with the MRC and DoH (England); and EPSRC Programme Grant EP/S032789/1. The views expressed are those of the authors and not necessarily those of the NHS, the NIHR, or the DoH. Scanning equipment was funded by an equipment grant from the Wellcome Trust.

References

(1). Schwarz SW. Ensuring a Safe, Reliable Supply of $^{99}Mo/^{99m}Tc$. J Nucl Med. 2016; 57(9):20N.

(2). Livieratos L. Technical pitfalls and limitations of SPECT/CT. Semin Nucl Med. 2015; 45(6):530–540. [PubMed: 26522394]

(3). Skerra A, Pfitzinger I, Pluckthun A. The functional expression of antibody Fv fragments in Escherichia coli: improved vectors and a generally applicable purification technique. Nat Biotechnol. 1991; 9(3):273–8.

(4). Waibel R, Alberto R, Willuda J, Finnern R, Schibli R, Stichelberger A, Egli A, Abram U, Mach JP, Pluckthun A, et al. Stable one-step technetium-99m labeling of His-tagged recombinant proteins with a novel Tc(I)-carbonyl complex. Nat Biotechnol. 1999; 17(9):897–901. [PubMed: 10471933]

(5). Alberto RS, Egli A, Schubiger AP. A novel organometallic aqua complex of technetium for the labeling of biomolecules: Synthesis of $[^{99m}Tc(OH_23(CO)3]^+$ from $[^{99m}TcO4]$ in aqueous solution and its reaction with a bifunctional ligand. J Am Chem Soc. 1998; 120:7987–7988.

Europe PMC Funders Author Manuscripts

(6). Torres Martin de Rosales, R, Blower, PJ. The role of ^{99m}Tc in the development of rhenium radiopharmaceuticalsTechnetium radiopharmaceuticals: status and prospective. Duatti, A, editor. IAEA; Vienna: 2008. 250–278.

(7). Schibli R, Schwarzbach R, Alberto R, Ortner K, Schmalle H, Dumas C, Egli A, Schubiger PA. Steps toward high specific activity labeling of biomolecules for therapeutic application: Preparation of precursor Re-188$(H_2O)_3(CO)_3$ $^+$ and synthesis of tailor-made bifunctional ligand systems. Bioconjugate Chem. 2002; 13(4):750–756.

(8). Chen WJ, Yen CL, Lo ST, Chen KT, Lo JM. Direct ^{99m}Tc labeling of Herceptin (trastuzumab) by ^{99m}Tc(I) tricarbonyl ion. Appl Radiat Isot. 2008; 66(3):340–5. [PubMed: 17996452]

(9). Chen, YL; Wu, CC; Lin, YC; Pan, YH; Lee, TW; Lo, JM. ^{99m}Tc(I)-tricarbonyl labeled histidine-tagged annexin V for apoptosis imaging. International Conference on Biomedical Imaging (ICBME) 2008, Proceedings; 2009. 1393–1396.

(10). Egli A, Alberto R, Tannahill L, Schibli R, Abram U, Schaffland A, Waibel R, Tourwe D, Jeannin L, Iterbeke K, et al. Organometallic ^{99m}Tc-aquaion labels peptide to an unprecedented high specific activity. J Nucl Med. 1999; 40(11):1913–7. [PubMed: 10565789]

(11). Ogawa K, Kawashima H, Kinuya S, Shiba K, Onoguchi M, Kimura H, Hashimoto K, Odani A, Saji H. Preparation and evaluation of Re-186/188-labeled antibody (A7) for radioimmunotherapy with rhenium(I) tricarbonyl core as a chelate site. Ann Nucl Med. 2009; 23(10):843–848. [PubMed: 19921351]

(12). Emberson LM, Trivett AJ, Blower PJ, Nicholls PJ. Expression of an anti-CD33 single-chain antibody by Pichia pastoris. J Immunol Methods. 2005; 305(2):135–151. [PubMed: 16139294]

(13). Tavare R, Torres Martin De Rosales R, Blower PJ, Mullen GE. Efficient site-specific radiolabeling of a modified C2A domain of synaptotagmin I with [^{99m}Tc(CO)3] $^+$: a new radiopharmaceutical for imaging cell death. Bioconjugate Chem. 2009; 20(11):2071–81.

(14). Badar A, Williams J, de Rosales RTM, Tavare R, Kampmeier F, Blower PJ, Mullen GED. Optimising the radiolabelling properties of technetium tricarbonyl and His-tagged proteins. EJNMMI Res. 2014; 4:14. [PubMed: 24606843]

(15). Tavare R, Williams J, Howland K, Blower PJ, Mullen GE. $[Re(CO)]^+$ labelling of a novel cysteine/hexahistidine tag: insights into binding mode by liquid chromatography-mass spectrometry. J Inorg Biochem. 2012; 114:24–7. [PubMed: 22687562]

(16). Orlova A, Nilsson FY, Wikman M, Widstrom C, Stahl S, Carlsson J, Tolmachev V. Comparative in vivo evaluation of technetium and iodine labels on an anti-HER2 affibody for single-photon imaging of HER2 expression in tumors. J Nucl Med. 2006; 47(3):512–9. [PubMed: 16513621]

(17). Frank R. The SPOT-synthesis technique. Synthetic peptide arrays on membrane supports-principles and applications. J Immunol Methods. 2002; 267:13–26. [PubMed: 12135797]

(18). Amartely H, Iosub-Amir A, Friedler A. Identifying protein-protein interaction sites using peptide arrays. J Visualized Exp. 2014; 93:e52097.

(19). Maisch D, Schmitz I, Brandt O. CelluSpots Arrays as an alternative to peptide arrays on membrane supports. Mini-Rev Org Chem. 2011; 8(2):132–136.

(20). Hofstrom C, Altai M, Honarvar H, Strand J, Malmberg J, Hosseinimehr SJ, Orlova A, Graslund T, Tolmachev V. Hahaha, Hehehe, Hihihi, Or Hkhkhk: Influence of position and composition of histidine containing tags on biodistribution of Tc-99m$(CO)_3$ $^+$-labeled affibody molecules. J Med Chem. 2013; 56(12):4966–4974. [PubMed: 23692562]

(21). Orlova A, Hofstrom C, Strand J, Varasteh Z, Sandstrom M, Andersson K, Tolmachev V, Graslund T. Tc-99m$(CO)3^+$-(HE)3-Z(IGF1R:4551), a new affibody conjugate for visualization of insulin-like growth factor-1 receptor expression in malignant tumours. Eur J Nucl Med Mol Imaging. 2013; 40(3):439–449. [PubMed: 23179942]

(22). Lindberg H, Hofstrom C, Altai M, Honorvar H, Wallberg H, Orlova A, Stahl S, Graslund T, Tolmachev V. Evaluation of a HER2-targeting affibody molecule combining an N-terminal HEHEHE-tag with a GGGC chelator for Tc-99m-labelling at the C terminus. Tumor Biol. 2012; 33(3):641–651.

(23). Hofstrom C, Orlova A, Altai M, Wangsell F, Graslund T, Tolmachev V. Use of a HEHEHE purification tag instead of a hexahistidine tag improves biodistribution of affibody molecules site-

Europe PMC Funders Author Manuscripts

Europe PMC Funders Author Manuscripts

specifically labeled with Tc-99m, In-111 and I-125. J Med Chem. 2011; 54(11):3817–3826. [PubMed: 21524142]

(24). Tolmachev V, Hofstrom C, Malmberg J, Ahlgren S, Hosseinimehr SJ, Sandstrom M, Abrahmsen L, Orlova A, Graslund T. HEHEHE-tagged affibody molecule may be purified by IMAC, is conveniently labeled with Tc-99m$(CO)_3^+$ and shows improved biodistribution with reduced hepatic radioactivity accumulation. Bioconjugate Chem. 2010; 21(11):2013–2022.

(25). Nawaz S, Mullen GED, Blower PJ, Ballinger JR. A ^{99m}Tc labelled scFv antibody fragment that binds to prostate specific membrane antigen. Nucl Med Commun. 2017; 38:666–671. [PubMed: 28598898]

(26). Kampmeier F, Williams JD, Maher J, Mullen GE, Blower PJ. Design and preclinical evaluation of a Tc-99m-labelled diabody of mAb J591 for SPECT imaging of prostate-specific membrane antigen (PSMA). EJNMMI Res. 2014; 4:10. [PubMed: 24593883]

(27). Bander NH, Trabulsi EJ, Kostakoglu L, Yao D, Vallabhajosula S, Smith-Jones P, Joyce MA, Milowsky M, Nanus DM, Goldsmith SJ. Targeting metastatic prostate cancer with radiolabeled monoclonal antibody J591 to the extracellular domain of prostate specific membrane antigen. J Urol. 2003; 170(5):1717–1721. [PubMed: 14532761]

(28). Smith-Jones PM, Vallabhajosula S, Navarro V, Bastidas D, Goldsmith SJ, Bander NH. Radiolabeled monoclonal antibodies specific to the extracellular domain of prostate-specific membrane antigen: Preclinical studies in nude mice bearing LNCaP human prostate tumor. J Nucl Med. 2003; 44(4):610–617. [PubMed: 12679407]

(29). Smith-Jones PM, Vallabahajosula S, Goldsmith SJ, Navarro V, Hunter CJ, Bastidas D, Bander NH. In vitro characterization of radiolabeled monoclonal antibodies specific for the extracellular domain of prostate-specific membrane antigen. Cancer Res. 2000; 60(18):5237–5243. [PubMed: 11016653]

(30). Chang SS, Reuter VE, Heston WDW, Bander NH, Grauer LS, Gaudin PB. Five different anti-prostatespecific membrane antigen (PSMA) antibodies confirm PSMA expression in tumor-associated neovasculature. Cancer Res. 1999; 59(13):3192–3198. [PubMed: 10397265]

(31). Strebe N, Guse A, Schungel M, Schirrmann T, Hafner M, Jostock T, Hust M, Muller W, Dubel S. Functional knockdown of VCAM-1 at the posttranslational level with ER retained antibodies. J Immunol Methods. 2009; 341(1-2):30–40. [PubMed: 19038261]

(32). Binkley SL, Leeper TC, Rowlett RS, Herrick RS, Ziegler CJ. $Re(CO)_3(H_2O)_3^+$ binding to lysozyme: structure and reactivity. Metallomics. 2011; 3(9):909–916. [PubMed: 21805003]

(33). Binkley SL, Ziegler CJ, Herrick RS, Rowlett RS. Specific derivatization of lysozyme in aqueous solution with $Re(CO)_3(H_2O)_3^+$. Chem Commun. 2010; 46(8):1203–1205.

(34). Cruickshank DR, Luyt LG. The development of organometallic OBOC peptide libraries and sequencing of N-terminal rhenium(I) tricarbonyl-containing peptides utilizing MALDI tandem mass spectrometry. Can J Chem. 2015; 93(2):234–243.

(35). Schibli R, Schubiger PA. Current use and future potential of organometallic radiopharmaceuticals. Eur J Nucl Med Mol Imaging. 2002; 29(11):1529–1542. [PubMed: 12397472]

(36). Lazarova N, Babich J, Valliant J, Schaffer P, James S, Zubieta J. Thiol-and thioether-based bifunctional chelates for the $\{M(CO)_3\}^+$ core (M = Tc, Re). Inorg Chem. 2005; 44(19):6763–6770. [PubMed: 16156635]

(37). He HY, Lipowska M, Christoforou AM, Marzilli LG, Taylor AT. Initial evaluation of new (Tc)-T-99m$(CO)_3$ renal imaging agents having carboxyl-rich thioether ligands and chemical characterization of $Re(CO)_3$ analogues. Nucl Med Biol. 2007; 34(6):709–716. [PubMed: 17707812]

(38). Makris G, Radford L, Gallazzi F, Jurisson S, Hennkens H, Papagiannopoulou D. Synthesis and evaluation of fac-Tc-99m/$Re(CO)_3^+$ complexes with a new (N,S,N) bifunctional chelating agent: The first example of a fac-$Re(CO)_3$(N,S,N-sst_2-ANT) complex bearing a somatostatin receptor antagonist peptide. J Organomet Chem. 2016; 805:100–107.

(39). Pietzsch HJ, Gupta A, Reisgys M, Drews A, Seifert S, Syhre R, Spies H, Alberto R, Abram U, Schubiger PA, et al. Chemical and biological characterization of technetium(l) and rhenium(I)

Europe PMC Funders Author Manuscripts

tricarbonyl complexes with dithioether ligands serving as linkers for coupling the $Tc(CO)_3$ and $Re(CO)_3$ moieties to biologically active molecules. Bioconjugate Chem. 2000; 11(3):414–424.

(40). Seifert S, Kunstler JU, Gupta A, Funke H, Reich T, Pietzsch HE, Alberto R, Johannsen B. Reactivity of technetium(I) thioether carbonyl complexes towards histidine - An EXAFS study in solution. Inorg Chim Acta. 2001; 322(1–2):79–86.

(41). Kannan R, Pillarsetty N, Gali H, Hoffman TJ, Barnes CL, Jurisson SS, Smith CJ, Volkert WA. Design and synthesis of a bombesin peptide-conjugated tripodal phosphino dithioether ligand topology for the stabilization of the fac-$[M(CO)_3]^+$ Core (M = ^{99m}Tc or Re). Inorg Chem. 2011; 50:6210–6219. [PubMed: 21591746]

(42). Matondo SOC, Mountford P, Watkin DJ, Jones WB, Cooper SR. Crown thioether chemistry - bis(1,4,7-trithiacyclononane)rhenium(II), the first homoleptic thioether complex of rhenium. J Chem Soc Chem Commun. 1995:161–162.

(43). Mullen GED, Fassler TF, Went MJ, Howland K, Stein B, Blower PJ. An investigation of C-S bond activation in transition metal crown thioether complexes using extended Huckel theory and electrospray mass spectrometry. J Chem Soc Dalton Trans. 1999:3759–3766.

(44). Mullen GED, Went MJ, Wocadlo S, Powell AK, Blower PJ. Electron transfer induced C-S bond cleavage in rhenium and technetium thioether complexes: Structural and chemical evidence for pi back-donation to C-S sigma* orbitals. Angew Chem Int Ed Engl. 1997; 36(11):1205–1207.

(45). Blower PJ, Kettle AG, O'Doherty MJ, Coakley AJ, Knapp FF. Tc-99m(V)DMSA quantitatively predicts Re-188(V)DMSA distribution in patients with prostate cancer metastatic to bone. Eur J Nucl Med. 2000; 27(9):1405–1409.

(46). Alberto R, Schibli R, Waibel R, Abram U, Schubiger AP. Basic aqueous chemistry of $M(OH_2)(CO)_3^+$ (M = Re, Tc) directed towards radiopharmaceutical application. Coord Chem Rev. 1999; 190:901–919.

(47). Herrick RS, Ziegler CJ, Sripothongnak S, Barone N, Costa R, Cupelo W, Gambella A. Preparation and characterization of rhenium (I) tricarbonyl dithiocarbamate compounds, $Re(CO)_3(S_2CNMe_2(L)$. J Organomet Chem. 2009; 694(24):3929–3934.

(48). Torres Martin de Rosales R, Finucane C, Mather SJ, Blower PJ. Bifunctional bisphosphonate complexes for the diagnosis and therapy of bone metastases. Chem Commun Cambridge U K. 2009:4847–4849.

(49). Jackson SN, Wang HYJ, Yergey A, Woods AS. Phosphate stabilization of intermolecular interactions. J Proteome Res. 2006; 5(1):122–126. [PubMed: 16396502]

(50). Woods AS, Ferre S. Amazing stability of the arginine-phosphate electrostatic interaction. J Proteome Res. 2005; 4(4):1397–1402. [PubMed: 16083292]

(51). Deyev SM, Vorobyeva A, Schulga A, Abouzayed S, Güntherd T, Garousi J, Konovalova E, Dinge H, Gräslund T, Orlova A, et al. Effect of a radiolabel biochemical nature on tumor-targeting properties of EpCAM-binding engineered scaffold protein DARPin Ec1. Int J Biol Macromol. 2020; 145:216–225. [PubMed: 31863835]

(52). Lindbo S, Garousi J, Åstrand M, Honarvar H, Orlova A, Hober S, Tolmachev V. Influence of histidine-containing tags on the biodistribution of ADAPT scaffold proteins. Bioconjugate Chem. 2016; 27:716–726.

(53). Vorobyeva A, Schulga A, Konovalova E, Güler R, Löfb lom J, Sandström M, Garousi J, Chernov V, Bragin O, Orlova A, et al. Optimal composition and position of histidine-containing tags improves biodistribution of ^{99m}Tc labeled DARPin G3. Sci Rep. 2019; 9:9405. [PubMed: 31253840]

(54). Torres Martin de Rosales R, Finucane C, Foster J, Mather SJ, Blower PJ. Re-188$(CO)_3$-dipicolylamine-alendronate: a new bisphosphonate conjugate for the radiotherapy of bone metastases. Bioconjugate Chem. 2010; 21(5):811–815.

Europe PMC Funders Author Manuscripts

Europe PMC Funders Author Manuscripts

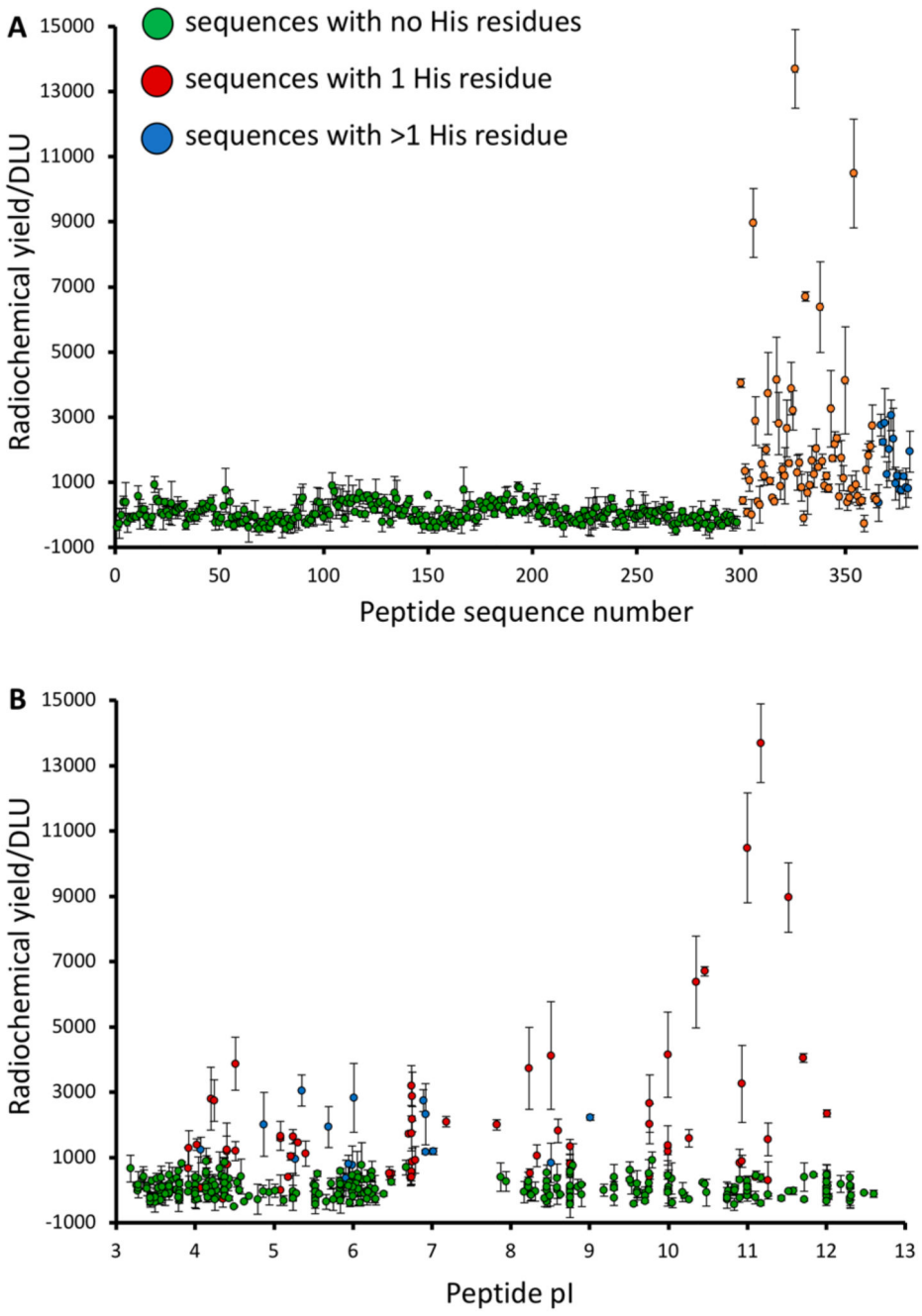

Figure 1. Initial observations from the STKS-1 array.

(A) Relative [^{99m}Tc][Tc(CO)$_3$]$^+$ labeling efficiency (DLU) of peptide sequences, categorized according to the number of His residues in the sequence; (B) Relationship between [^{99m}Tc][Tc(CO)$_3$] $^+$ labeling efficiency and isoelectric point. GREEN = no His residues; RED = 1 His residue; BLUE = 2 or more His residues.

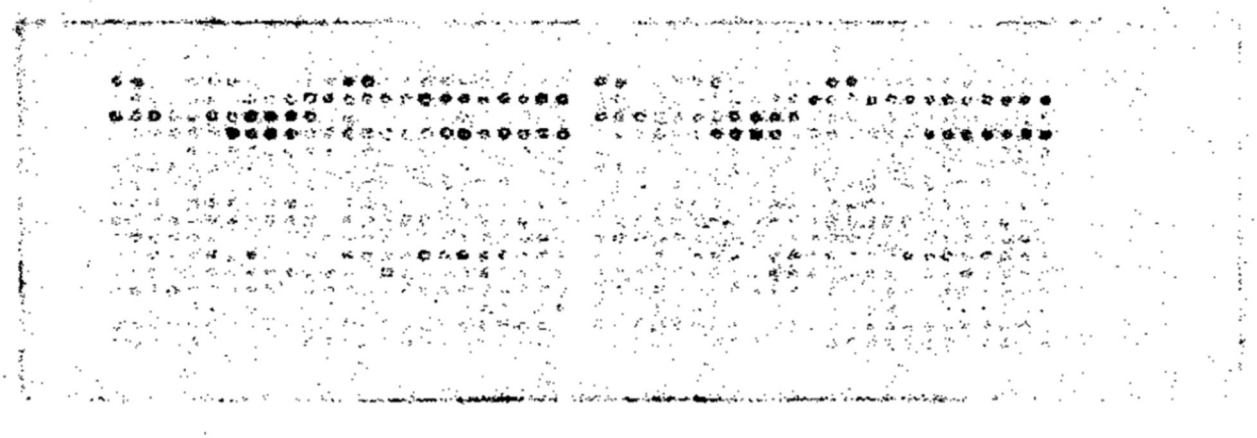

Figure 2. Typical digital autoradiograph of the His-tag array after incubation with [^{99m}Tc][Tc(CO)$_3$]$^+$ in phosphate buffer for 15 min.

Images obtained after 30, 60, and 120 min incubation are shown in SI Figure S2. The layout of amino acid sequences in the array can be seen in SI Tables S3–S4.

Europe PMC Funders Author Manuscripts

Europe PMC Funders Author Manuscripts

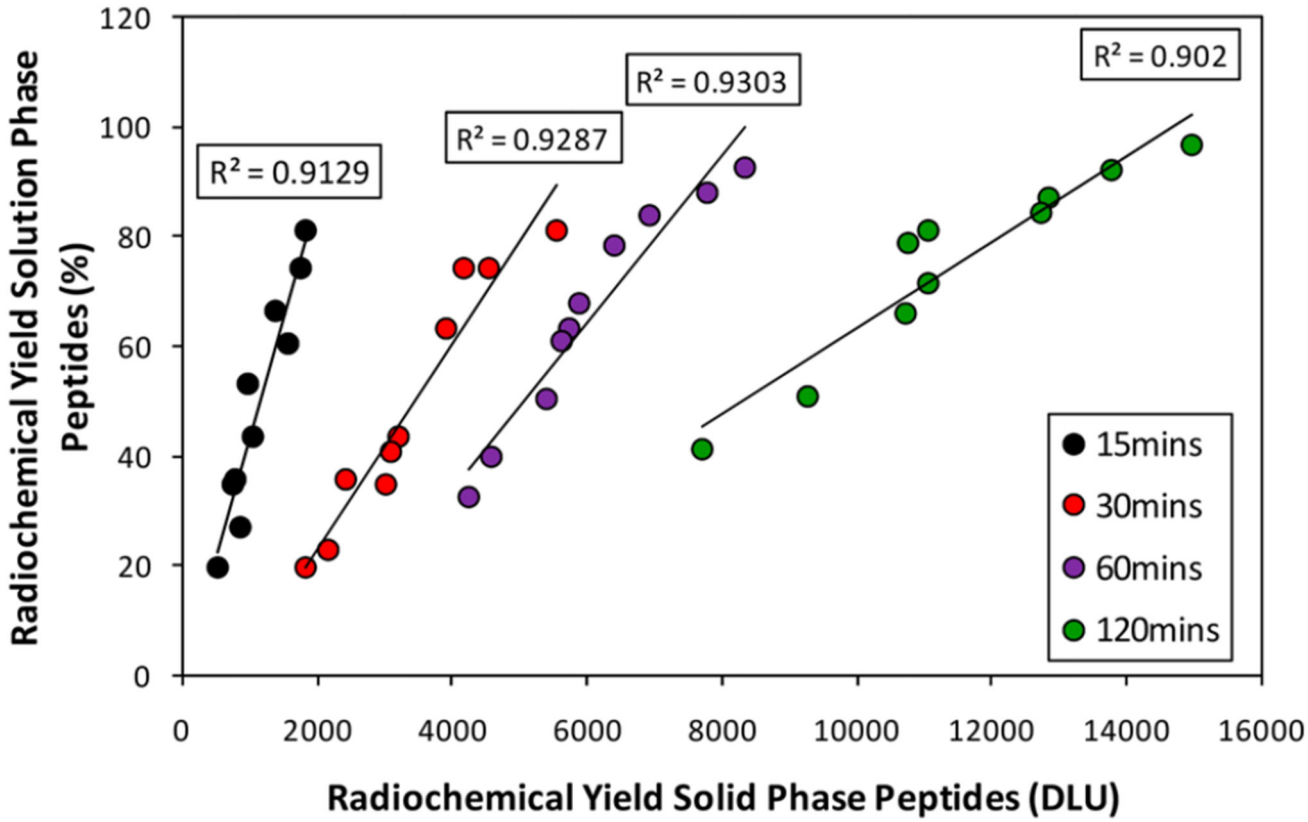

Figure 3. Correlation between the radiochemical yield of ten sequences selected from the His-tag array in solution and on solid phase after 15, 30, 60, and 120 min incubation with $[^{99m}Tc][Tc(CO)_3]^+$.

The sequences selected were LAAALEHHHHHH, CKLA-AALEHHHHHH, LAAALEHAHAHA, CKLAAALEHAHAHA, LAAALEHHHH, CKLAAALEHHHH, LAAALEHAHA, CKLA-AALEHAHA, LAAALEHAAH, CKLAAALEHAAH.

Europe PMC Funders Author Manuscripts
Europe PMC Funders Author Manuscripts

Europe PMC Funders Author Manuscripts

Europe PMC Funders Author Manuscripts

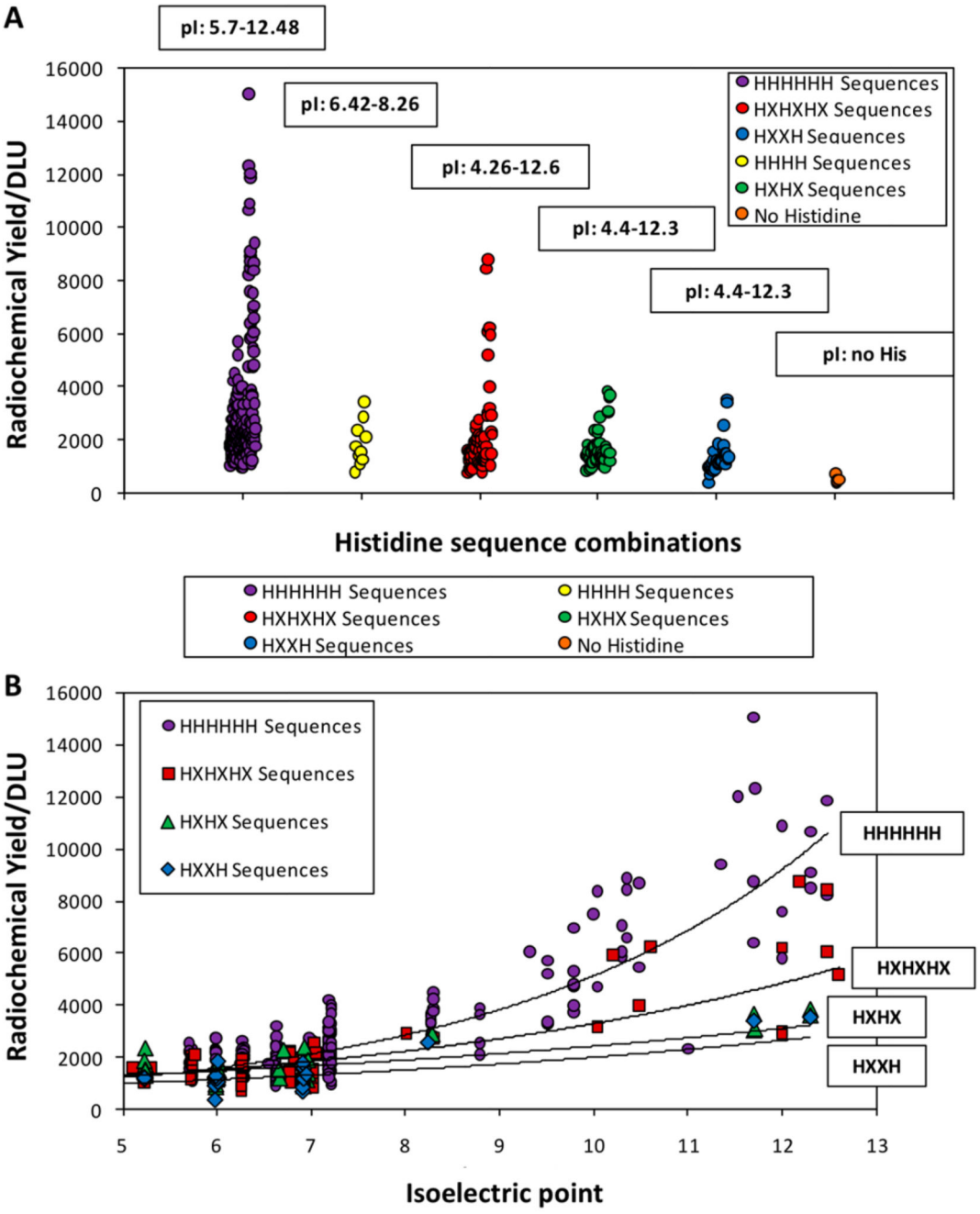

Figure 4.

A. Effect of interrupting His tag sequences with other amino acids (X): HHHHHH (purple), HHHH (yellow), HXHXHX (red), HXHX (green), and HXXH (blue). B. relationship between pI and radiochemical yield plotted separately for sequences with HHHHHH (purple), HXHXHX (red), HXHX (green), and HXXH (blue). Lines correspond to a monoexponential fit for each group.

Europe PMC Funders Author Manuscripts

Europe PMC Funders Author Manuscripts

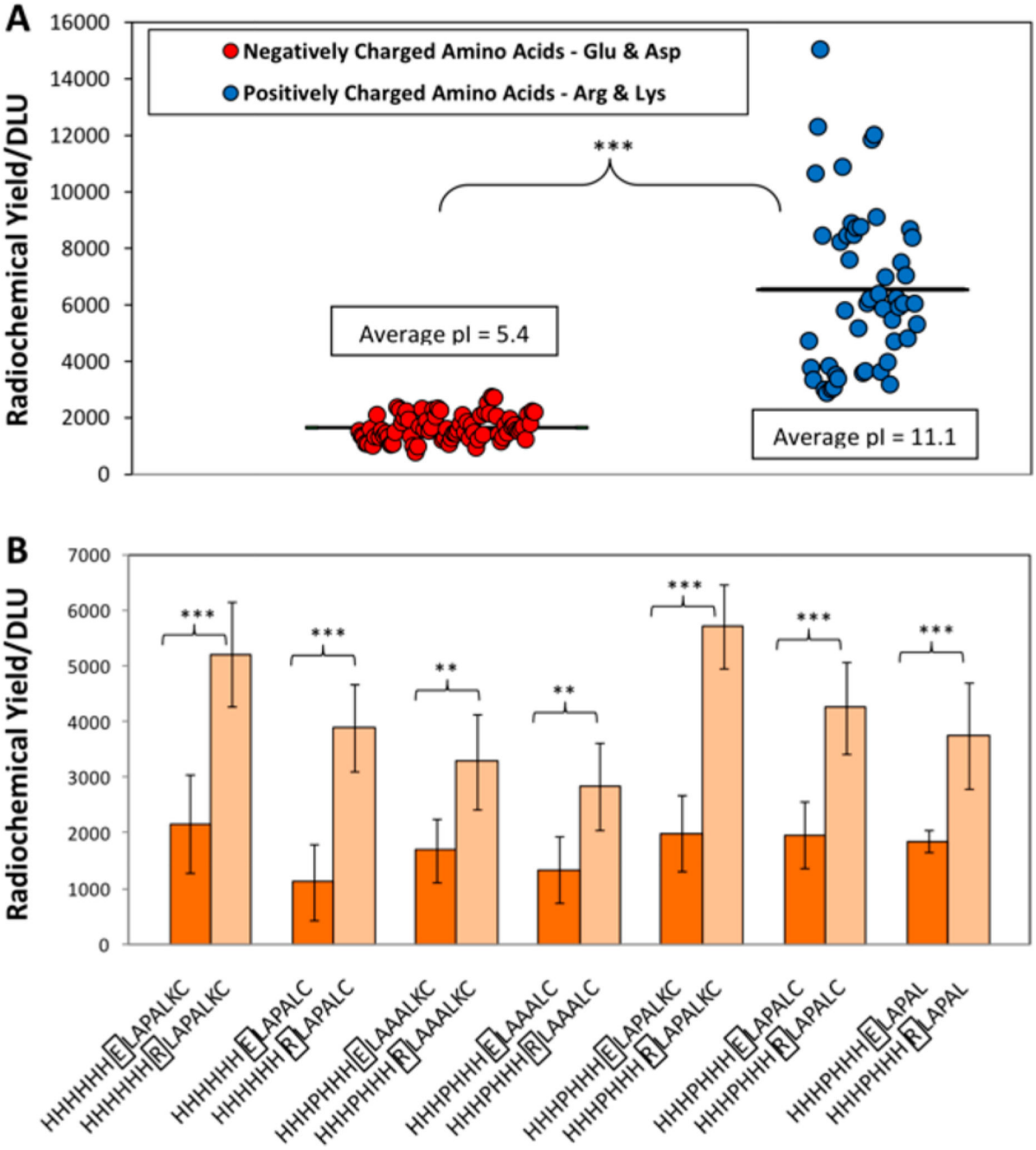

Figure 5. Effect of positively and negatively charged amino acids on [“mTc][Tc(CO)3]$^{+}$ labeling efficiency.

A. Comparison of the radiolabeling of all peptide sequences with at least 2 negatively charged amino acids (Glu and/or Asp, mean pI 11.1) and at least 2 positively charged amino acids (Arg and/or Lys, mean pI 5.4). The black lines represent the average radiochemical yield for each group. B. Effect on labeling efficiency of paired “point mutation” replacing Glu (E) with Arg (R) in the seven otherwise identical His tag variants where such comparison was possible. ***$p < 0.001$; **$p < 0.01$.

Europe PMC Funders Author Manuscripts

Europe PMC Funders Author Manuscripts

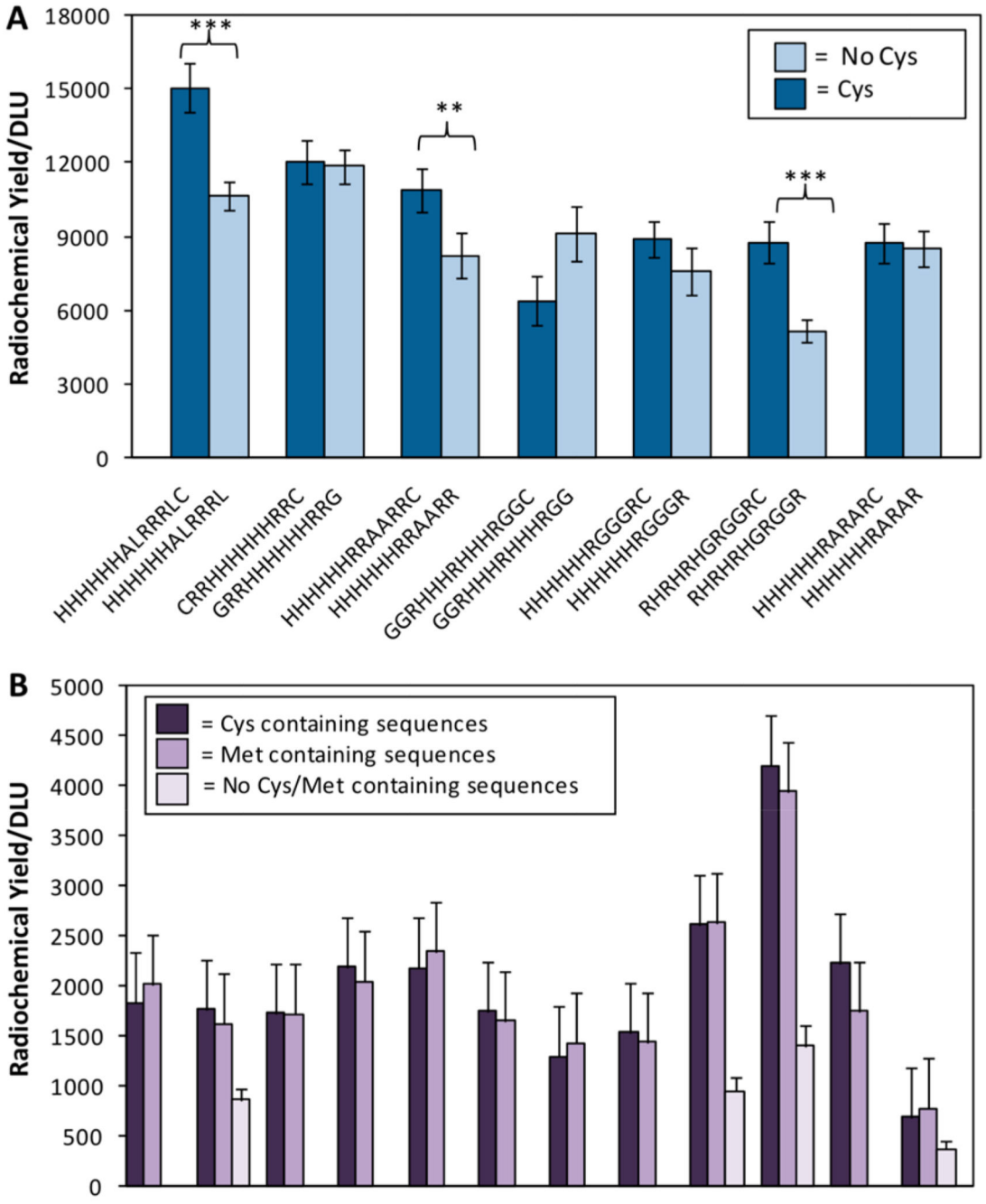

Figure 6. Effect of cysteine and methionine.

A. Radiochemical yield for the seven Cys-containing sequences appearing among the ten best labeling sequences, compared to otherwise identical partner “mutants” in which Cys was deleted or substituted. In all but one pair, the Cys-containing sequence showed higher labeling efficiency (*** $p < 0.001$; ** $p < 0.05$). B. Comparison of labeling efficiency of identical peptide sequences in which a Cys residue is replaced by a Met amino acid. For four of the pairs, the corresponding sequence with neither Cys or Met is also included.

Europe PMC Funders Author Manuscripts

Europe PMC Funders Author Manuscripts

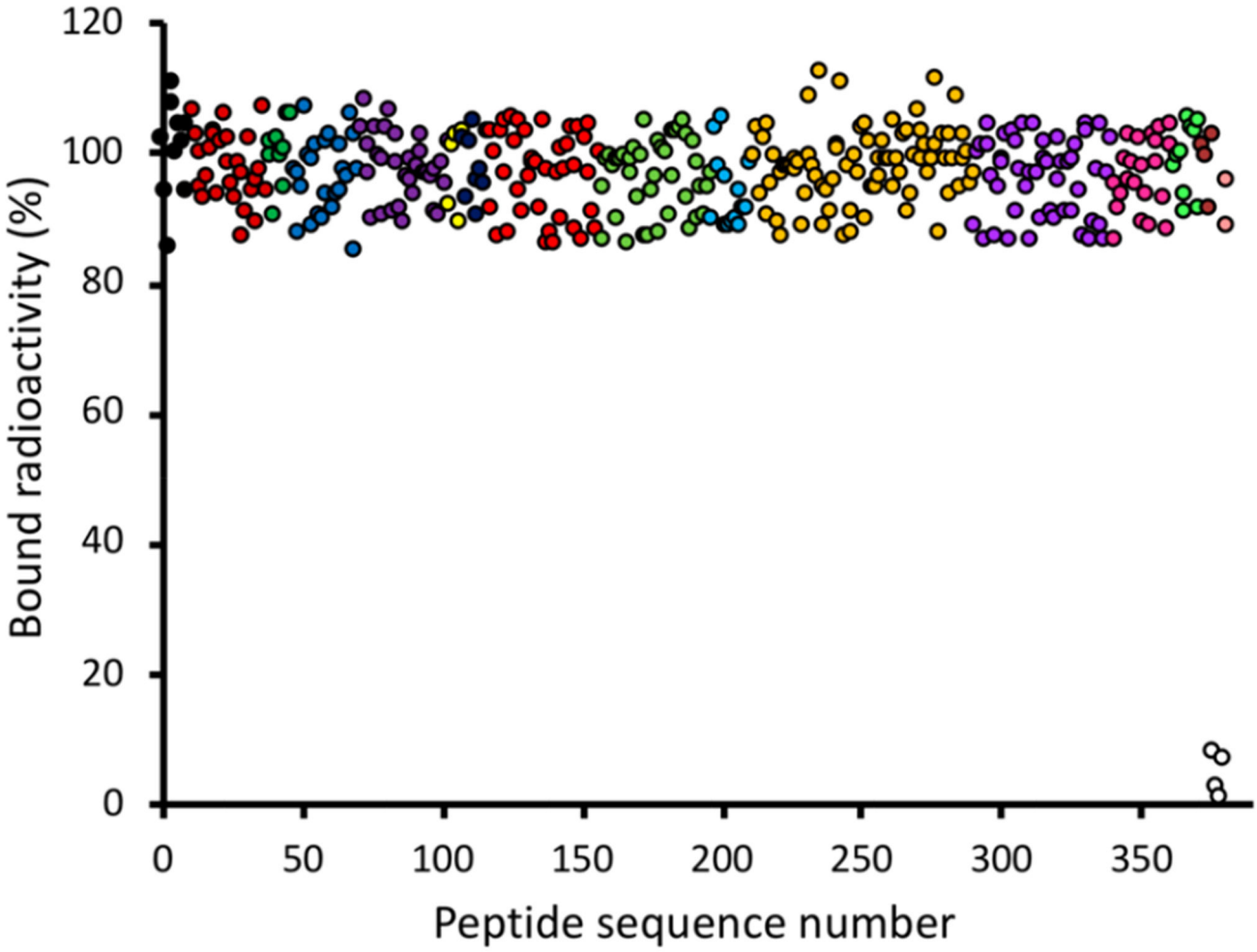

Figure 7. Radiochemical stability of [^{99m}Tc][Tc(CO)3]$^{+}$-labeled (in PBS) sequences after exposure to human serum for 24 h.

Sequence categories and color coding are as for SI Figure S3. Only His-free peptide spots and peptide-free spots (white symbols) lost a significant fraction of their radioactivity. Similar data are shown in Supporting Information for exposure to serum for 1 and 2 h (Figure S20), and for incubation with PBS (Figure S18) and histidine and cysteine solution (Figure S22), along with a legend showing color coding of peptide categories and the images used to obtain these data (Figures S19, S17, S21).

Europe PMC Funders Author Manuscripts

Europe PMC Funders Author Manuscripts

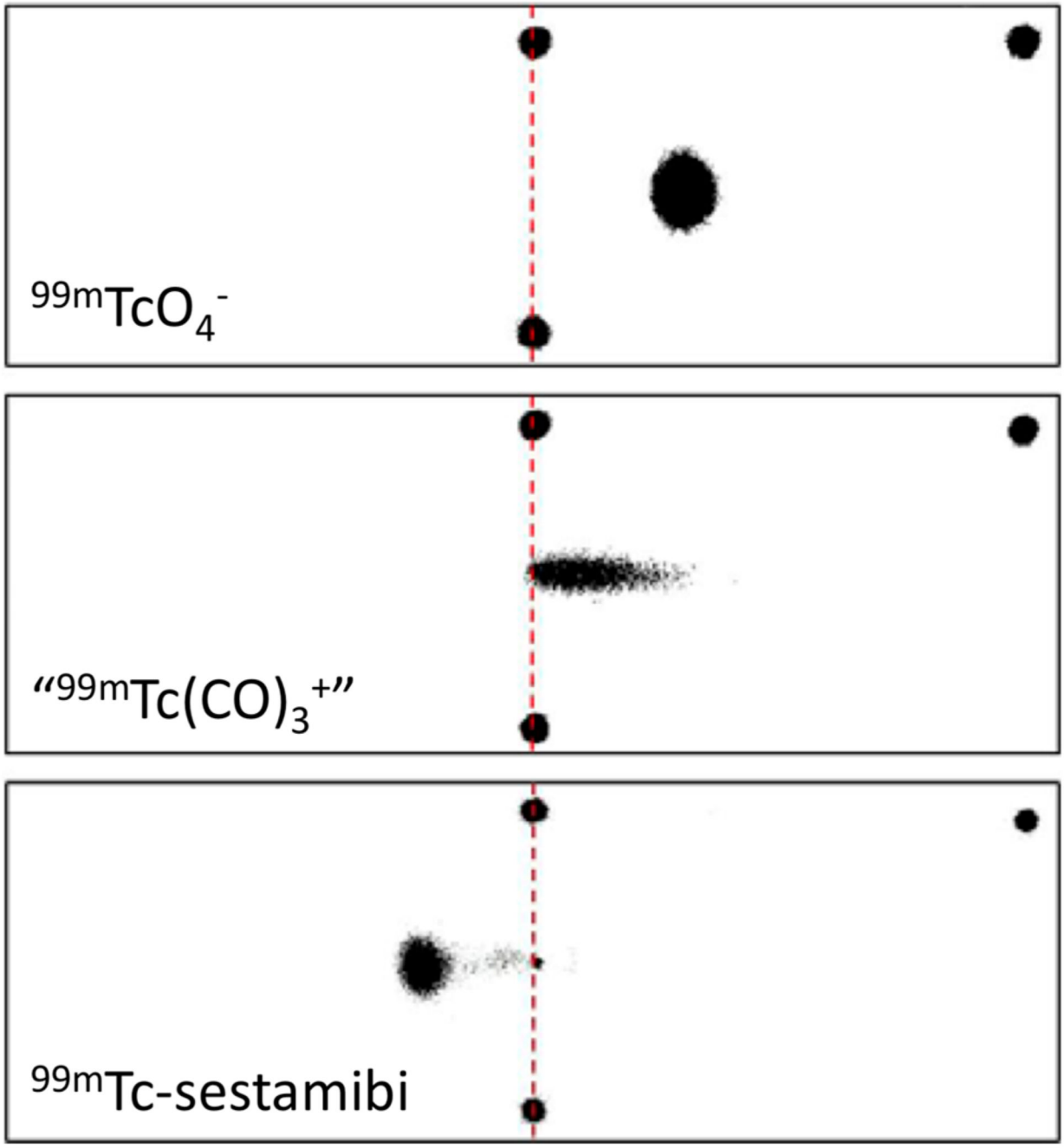

Figure 8. Phosphor images obtained from electrophoresis of [^{99m}Tc][TcO4]$^-$ (top), [^{99m}Tc]-sestamibi (middle), and "[^{99m}Tc]-[Tc(CO)$_3$]$^+$" in PBS (pH 7.4).

The two black spots joined by a red dashed line represent the starting point of the radioactive complexes, and the black spot at the top right indicates the position of the anode. Electrophoresis results in citrate buffer at pH 5.1, tris-HCl buffer at pH 7.4, and tris-HCl buffer at pH 8.8 are shown in SI Figure S26).

Europe PMC Funders Author Manuscripts

Europe PMC Funders Author Manuscripts

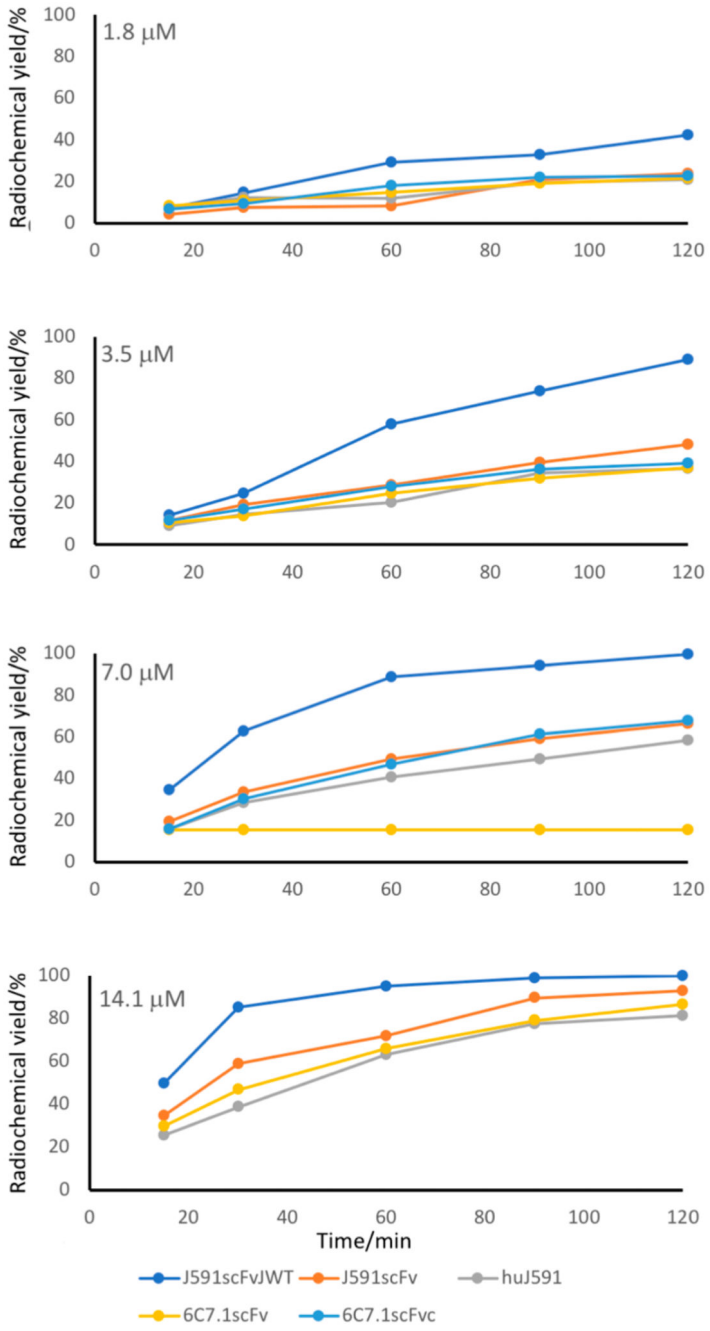

Figure 9. Labeling efficiency of five His-tagged proteins with [^{99m}Tc(CO)3]$^{+}$ in PBS during 120 min at 37 °C, at protein concentrations from 1.8 to 14.1 μM.

Only J591scFvJWT (blue line) contains an optimized His-tag. There are no data for the highest and the highest two concentrations, respectively, of 6C7.1scFv and 6C7.1scFvCys because restricted quantities were available. Data for the extended concentration range (0.9–28 μM) are shown in SI Figure S32.

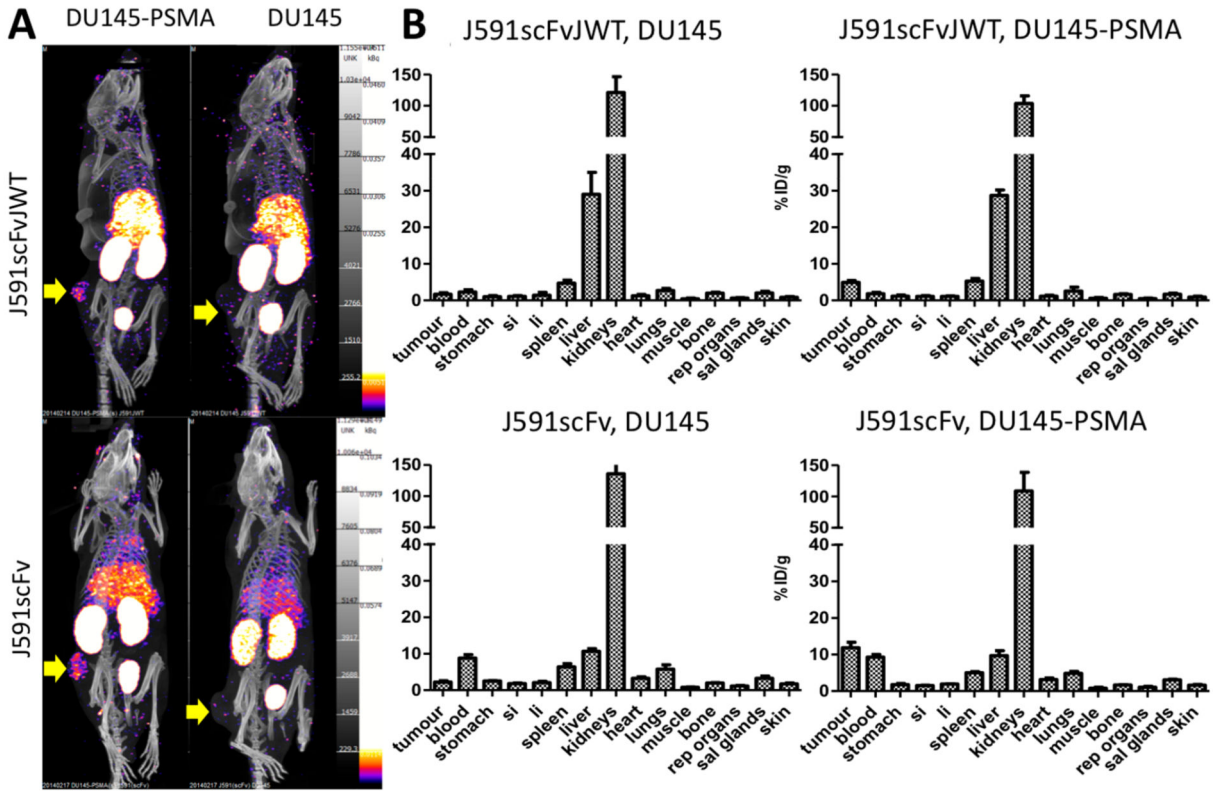

Figure 10. ***In vivo*** **biodistribution and tumor targeting of [^{99m}Tc][Tc(CO)$_3$]$^+$-J591scFvJWT and [^{99m}Tc][Tc(CO)$_3$]$^+$-J591scFv' showing specific uptake in PSMA-expressing tumor.**

A. Example SPECT-CT images (75–90 min post-injection). B. *Ex vivo* biodistribution (90 min post-injection) of mice bearing DU145 tumor (non-PSMA expressing, indicated by yellow arrows, right images) and DU145-PSMA tumor (PSMA expressing, indicated by yellow arrows, left images) after administration of [^{99m}Tc][Tc(CO)$_3$]$^+$-J591scFvJWT (top images) or [^{99m}Tc][Tc(CO)$_3$]$^+$-J591scFv (bottom images). si = small intestine; li = large intestine; rep = reproductive; sal = salivary. Error bars represent standard deviation, n = 4 per group.

Europe PMC Funders Author Manuscripts
Europe PMC Funders Author Manuscripts

Europe PMC Funders Author Manuscripts

Europe PMC Funders Author Manuscripts

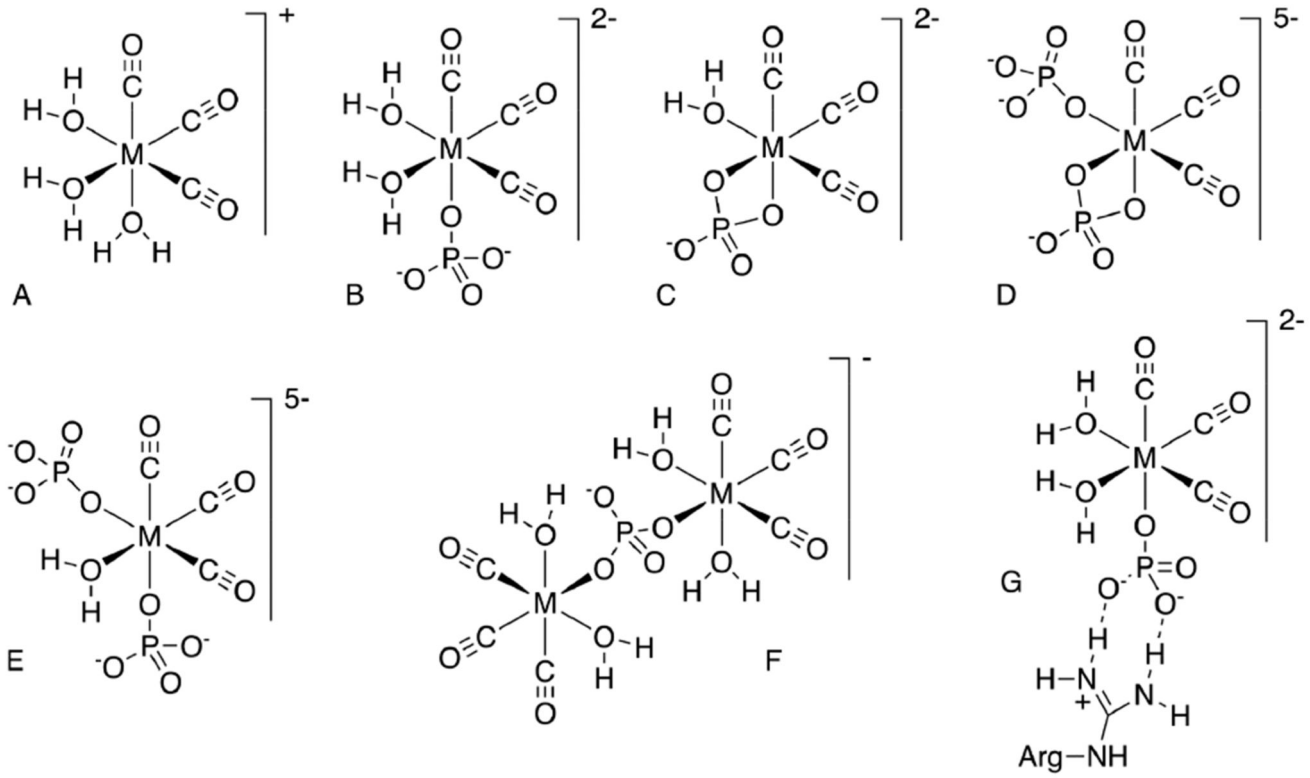

Figure 11.

Presumed structure of the cationic technetium and rhenium $[M(CO)_3]^+$ aqua complex (A), and possible structures of $[M(CO)_3]^+$ complexes with phosphate, that could give rise to additional ^{31}P NMR resonances and negatively charged complexes. As well as mononuclear species such as (B-E), dinuclear species such as (F) and higher nuclearity species may be expected to exist in bulk solutions used for NMR, while at trace concentrations of Tc and Re present in the radioactive solutions, only mononuclear species would be expected to contribute significantly to the speciation. Also shown, (G) is a putative “salt bridge” interaction between an arginine side chain and coordinated phosphate.